Cell Stem Cell

Short article

Human airway submucosal gland organoids to study respiratory inflammation and infection

Graphical abstract

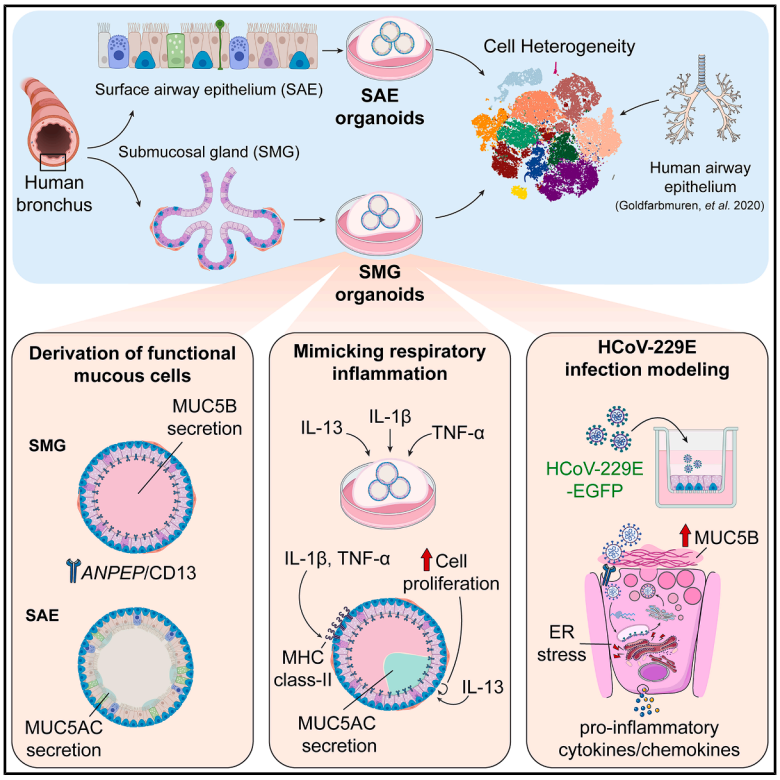

Highlights

- Development of human bronchus tissue-derived submucosal gland organoids
- ANPEP/CD13 is a specific marker for glandular secretory cells
- COPD-related cytokines elicit distinct inflammatory responses
- Human alpha-coronavirus 229E primarily infects glandular secretory cells

Authors

Lin Lin, Carla Pou Casellas, Antonella F. M. Dost, ..., Volker Thiel, Johan H. van Es, Hans Clevers

Correspondence

linlin@sibcb.ac.cn (L.L.), h.clevers@hubrecht.eu (H.C.)

In brief

Lin and Pou Casellas et al. established human airway submucosal gland (SMG) organoid cultures that capture region-specific mucous cells and viral infection responses. These SMG organoids provide a new platform to investigate airway regeneration, inflammation, and viral infections, offering insights into respiratory (patho-)physiology beyond the surface epithelium.

Lin et al., 2025, Cell Stem Cell *32*, 1170–1182
July 3, 2025
https://doi.org/10.1016/j.stem.2025.05.013

CellPress

CellPress
OPEN ACCESS

Cell Stem Cell

Short article

Human airway submucosal gland organoids to study respiratory inflammation and infection

Lin Lin,[1,2,3,4,12,*] Carla Pou Casellas,[1,3,5,12] Antonella F.M. Dost,[1,3] Harry Begthel,[1,3] Jeroen Korving,[1,3] Stieneke van den Brink,[1,3] Talya Dayton,[6] Matthijs F.M. van Oosterhout,[7] Niels Smakman,[8] Lisa Thomann,[9,10,11] Volker Thiel,[9,10,11] Johan H. van Es,[1,3] and Hans Clevers[1,3,4,13,14,*]

[1]Hubrecht Institute, Royal Netherlands Academy of Arts and Sciences (KNAW), University Medical Center, Utrecht 3584 CT, the Netherlands
[2]Key Laboratory of Cell Biology, Shanghai Institute of Biochemistry and Cell Biology, Center for Excellence in Molecular Cell Science, Chinese Academy of Sciences, University of Chinese Academy of Sciences, Shanghai 200031, China
[3]Oncode Institute, Hubrecht Institute, Utrecht 3584 CT, the Netherlands
[4]Princess Maxima Center for Pediatric Oncology, Utrecht 3584 CS, the Netherlands
[5]Department of Nephrology and Hypertension, University Medical Center Utrecht (UMCU), Utrecht 3508 GA, the Netherlands
[6]European Molecular Biology Laboratory (EMBL) Barcelona, Tissue Biology and Disease Modelling, Barcelona 08003, Spain
[7]Department of Pathology, DNA Pathology, St Antonius ILD Center of Excellence, St Antonius Hospital, Nieuwegein 3435 CM, the Netherlands
[8]Department of Surgery, Diakonessenhuis Hospital, Utrecht 3582 KE, the Netherlands
[9]Institute of Virology and Immunology (IVI), Bern and Mittelhäusern, Switzerland
[10]Department of Infectious Diseases and Pathobiology, Vetsuisse Faculty, University of Bern, Bern 3012, Switzerland
[11]Multidisciplinary Center for Infectious Diseases (MCID), University of Bern, Bern 3012, Switzerland
[12]These authors contributed equally
[13]Present address: Institute of Human Biology (IHB), Pharma, Research and Early Development (pRED) of F. Hoffmann-La Roche Ltd, Basel, Switzerland
[14]Lead contact
*Correspondence: linlin@sibcb.ac.cn (L.L.), h.clevers@hubrecht.eu (H.C.)
https://doi.org/10.1016/j.stem.2025.05.013

SUMMARY

The human airway lining consists of two physiologically distinct compartments: the surface airway epithelium (SAE) and the submucosal glands (SMGs). Despite their critical role, the SMGs have remained largely overlooked in airway *in vitro* modeling of respiratory inflammation and infection. In this study, we leverage long-term cultured organoids derived separately from SAE and SMGs to investigate their unique physiological characteristics. Single-cell RNA sequencing (scRNA-seq) analysis confirms that these organoid models accurately replicate the cellular heterogeneity inherent to each tissue type. Specifically, SMG organoids are enriched in MUC5B-producing mucous cells and also generate alpha-smooth muscle actin (αSMA)-expressing myoepithelial cells. *ANPEP*/CD13 specifically marks SMG secretory cells. Exposure to cytokines elicits distinct inflammatory transcriptomic responses in SMG secretory cells. Infection assays with human alpha-coronavirus 229E (HCoV-229E) reveal the selective vulnerability of CD13-positive secretory cells, triggering an unfolded protein response. These findings broaden the utility of airway organoids for modeling respiratory (patho-)physiology.

INTRODUCTION

Human airways are lined by two distinct epithelial structures: the ciliated epithelium, which covers the surface areas of the respiratory tract, and the mucus-producing glands embedded within the submucosal space of all cartilaginous airways.[1] The surface airway epithelium (SAE) consists of four major cell types: basal, ciliated, club, and MUC5AC-producing mucous cells. This layer acts as a physical barrier and facilitates mucociliary clearance. By contrast, airway submucosal glands (SMGs), predominantly located along the trachea and large bronchi, comprise mainly MUC5B-producing mucous, serous, basal, and myoepithelial cells (MECs).[2–5] SMGs are responsible for the secretion of mucus and various antimicrobial peptides, which are essential for maintaining airway humidity and protecting against pathogens.[6,7] This cellular heterogeneity not only contributes to the SMG's primary role in mucus secretion but also to its intricate response to inflammatory stimuli and pathogens.

Recent studies have shown that SMGs contribute to the repair and regeneration of airway epithelium following injury in mouse models, suggesting a potential reservoir of progenitor cells capable of differentiating into multiple airway cell types.[8,9] This regenerative capacity implicates SMGs in both health and disease, particularly in conditions such as chronic obstructive

pulmonary disease (COPD), where airway remodeling and chronic inflammation are prevalent. Indeed, SMG hypertrophy is recognized as one of the main pathophysiological changes in COPD airways, causing mucus hypersecretion, airway obstruction, and exacerbation of lung injury.[10,11]

Despite their importance, there has been no robust *in vitro* model of SMGs from adult tissues beyond short-lived explant cultures from human or animal models.[12–15] Organoid-based disease modeling of human airways has predominantly focused on the more accessible SAE.[16,17] Given the SMG's essential role in mucus production and host defense, we established human organoids derived from primary bronchus tissues from both SAE and SMG regions.

RESULTS

Establishment and characterization of human bronchus SMG organoids

To isolate SMGs from human upper airways, we refined existing airway tissue processing protocols.[17,18] A two-step enzymatic digestion first removed the SAE from the bronchus (Figure 1A), followed by the release of SMGs from submucosal muscle fibers. SAE cell sheets and SMG glandular clusters were then cultured separately in tailored media (Figure 1B). We established SAE and SMG organoids from 7 independent donors (Figures 1C and S1A) and passaged them every 21–28 days for at least 8 passages (Figure S1B). The media supported both basal cell expansion and spontaneous differentiation. By day 28, organoids exhibited the relevant differentiated cell types: SMG organoids contained PAS+ and MUC5B+ mucous cells, while SAE organoids were predominantly composed of basal cells, ciliated cells, and the rarer mucus-producing cells (Figure 1D). Consistent with native tissue, SMG mucous cells predominantly expressed MUC5B, whereas SAE mucous cells expressed both MUC5AC and MUC5B (Figure 1E).[19,20]

Single-cell characterization of human SMG and SAE organoid cultures

To compare the SMG and SAE organoid models with their tissue counterparts, we performed single-cell RNA sequencing (scRNA-seq) of both organoid cultures on day 28 of passage 4 and integrated this dataset with a previously published human airway epithelium tissue dataset.[21] This combined dataset included 1,315 SMG organoid cells, 1,120 SAE organoid cells, and 36,248 tissue cells, yielding a total of 38,683 cells (Figure 2A). Based on reference tissue markers,[2,3,21–23] organoid-derived cells clustered closely with their tissue counterparts (Figures 2B and 2C; Table S1). Both SAE and SMG organoids contained differentiating basal cells (*TP63*^{low} and *IL33*$^{+}$) (SAE: 27.1%; SMG: 13.9%) and *KRT8*^{high} intermediate cells (SAE: 14.9%; SMG: 19.5%) (Figures S2A–S2C). Distinctly, SMG organoids were comprised of SMG basal cells (44.3%) (*KRT14*$^{+}$ and *G0S2*$^{+}$) and SMG secretory cells (4.1%) (*MUC5B*$^{+}$ and *DMBT1*$^{+}$). By contrast, SAE basal cells (*TP63*$^{+}$ and *MMP10*$^{+}$), SAE secretory cells (*MUC5AC*$^{+}$ and *CEACAM5*$^{+}$), and club cells (*SCGB1A1*$^{+}$) were primarily found in SAE organoids (Figures 2D and S2A–S2C; Table S1). Notably, pulmonary neuroendocrine cells (PNECs) were not captured in the organoid cultures. Given the rarity of PNECs *in vivo*, additional signaling pathways might be required in the organoid model to trigger PNEC differentiation. Indeed, a previous study in lung neuroendocrine neoplasms has shown that WNT activator and basic fibroblast growth factor are required to support neuroendocrine tumor organoid outgrowth.[24] Nevertheless, differentiated cell types in both models exhibited mature transcriptional profiles (Figure S2D).

SMG and SAE tissues harbor distinct basal and secretory populations. By analyzing differentially expressed genes (DEGs) between SMG and SAE basal cell clusters, we confirmed higher expression of previously reported markers (*VIM*, *SOX9*, *FOXC1*, and *KRT14*) in SMG basal cells[21,25,26] and enrichment of *MMP10* and *WNT4* in SAE basal cells (Figure S2E).[22,27] Notably, the presence of SMG organoid-derived cells within the SAE basal cell cluster likely reflects the shared transcriptional signatures. Despite this apparent overlap, these "mis-clustered" SMG cells retained unique transcriptional profiles with low expression of SAE-specific basal markers (*GJB2*, *MMP10*, *WNT4*, and *CAVIN2*) (data not shown).

Comparison of SMG and SAE secretory cells revealed consistent lineage-specific expression patterns. SMG secretory cells, both organoid- and tissue-derived, expressed higher levels of *DMBT1*, *FOLR1*, *PROM1*, and *MUC5B*, while SAE secretory cells preferentially expressed *MUC5AC*, *KLK11*, and *CEACAM5* (Figure S2F).[22,28] These findings align with prior human airway cell atlas studies and reinforce the molecular distinction between SMG and SAE lineages. Within the SMG secretory compartment, serous cells, a subset of acinar cells producing antimicrobial peptides, were not readily detected in organoids. RT-qPCR analysis of serous cell markers (*PRR4*, *LTF*, and *LYZ*)[22,29] revealed expression at P0 but a marked decline by P4/5 (Figure S2G), suggesting serous cell loss during *in vitro* expansion, potentially due to missing niche cues.

A defining feature of the SMG is the presence of MECs. These specialized epithelial cells are located at the interface between the glandular epithelium and the underlying basement membrane. MECs express smooth muscle markers such as smooth muscle actin (α-SMA) and myosin, enabling their contractile function to expel glandular secretions into the airway lumen.[1,30–32] Additionally, MECs have been shown to function as reserve stem cells to repair tracheal SAE following severe injury in mouse models.[8,9] Employing an MEC cell score based on previously reported markers,[8,9,23,33] we identified a small MEC population within the SMG basal cell cluster (n = 62), comprising 2.2% of SMG organoid cells and 3.1% of SMG tissue cells but absent in SAE (Figure 2E). These cells retained the expression of smooth muscle cell markers (*ACTA2*, *TAGLN*, *ACTG2*, and *PCP4*). By contrast, the few SAE-derived basal cells that were assigned to the SMG basal cluster (0.98%) only expressed basal cell (*KRT14* and *KRT5*) and cell-cell adhesion (*FHOD3* and *LAMA1*) markers (Figure 2F). The presence of these MECs in SMG organoids was further confirmed by staining of α-*SMA* in organoids derived from an independent donor (Figure 2G).

Next, we sought to understand the unique secretory functions of SMGs. To facilitate the targeted enrichment of SMG secretory cells, we assayed the differential expression of cell surface genes and identified *ANPEP* (CD13) as one of the highly enriched surface markers in SMG secretory cells (Figures 2H and S2H).

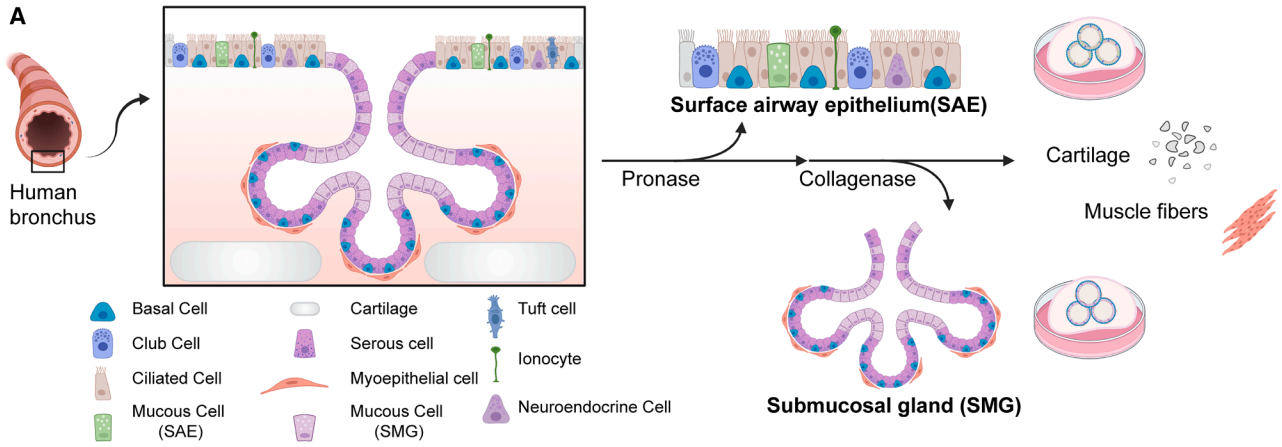

B

Culture media composition

	SMG	SAE
Basal culture medium	+	+
Noggin	+	+
A-83-01	+	+
N-Acetylcysteine	+	+
FGF-10	+	+
FGF-7	+	-
SB202190	+	-
Nicotinamide	+	-

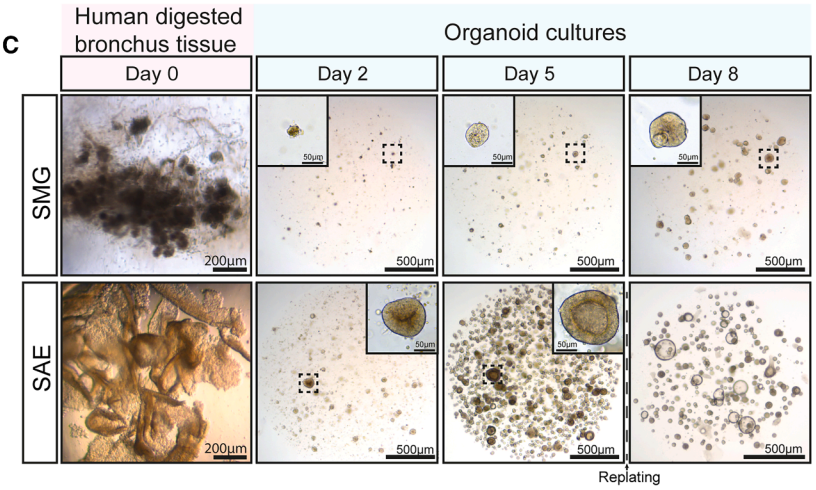

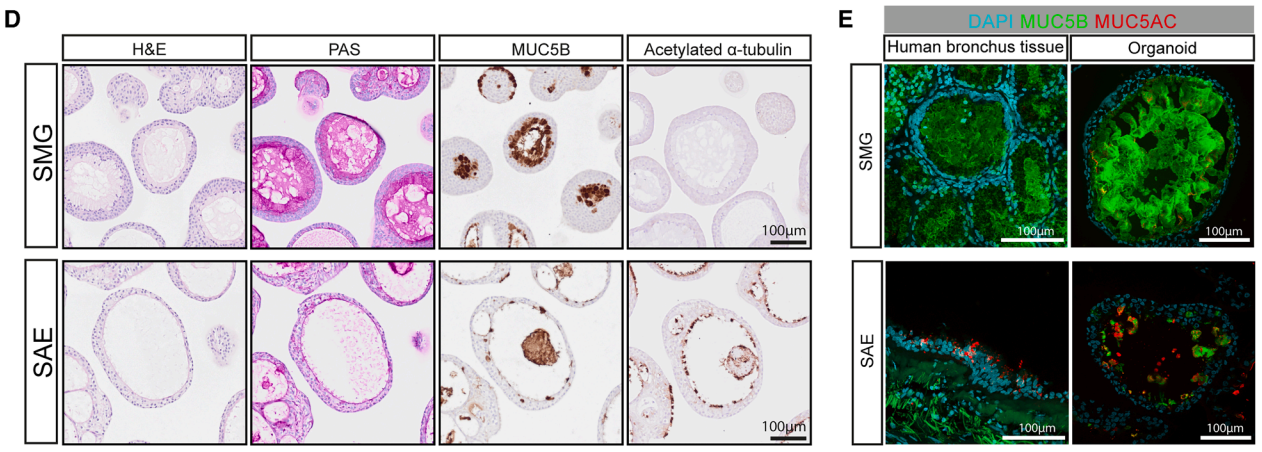

Figure 1. Establishment and characterization of human bronchus SMG organoids

(A) Schematic of tissue processing procedures to isolate SAE and SMG compartments from human bronchus tissue.

(B) Culture media compositions for SAE and SMG organoids.

(C) Time-lapse bright-field images of SMG and SAE organoids established from human bronchus tissues (donor: #OHLT019). Note: SAE organoids were replated on day 7 to support continued growth and spatial expansion.

(D) H&E staining, goblet cells (PAS), SMG-specific mucous cells (MUC5B), and SAE ciliated cells (acetylated α-tubulin) in SMG and SAE organoids detected by immunohistochemistry (IHC) staining (donor: #OHLT019).

(E) Representative immunofluorescence staining of SMG-specific mucous cells (MUC5B, green), SAE-specific mucous cells (MUC5AC, red), and nuclei (DAPI, cyan) in human bronchus tissue and organoids (donor: #0704).

See also Figure S1.

CellPress
OPEN ACCESS

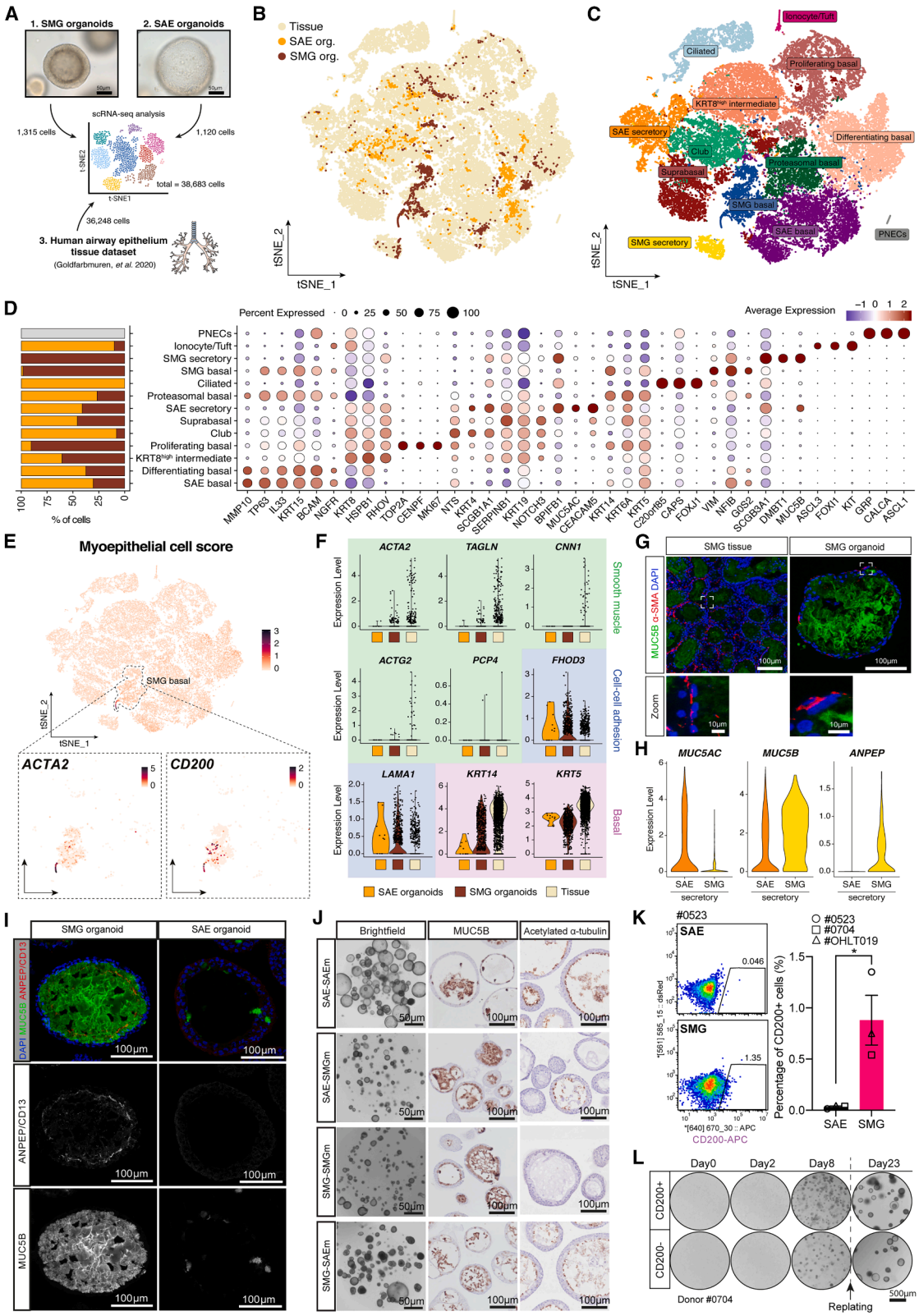

(legend on next page)

CD13 localized to the apical surface of SMG tissues and organoids but was absent in SAE (Figures 2I and S2I). Fluorescence-activated cell sorting (FACS) analysis showed that

$CD13^+$ cells (0.5%–4%, donor variation observed) were exclusive to SMG organoids and co-expressed MUC5B (Figure S2J). RT-qPCR analysis further demonstrated enrichment of glandular secretory cell markers (*MUC5B*, *LTF*, and *LYZ*) and decreased expression of basal cell markers (*KRT14*, *KRT5*, and *TP63*) in $CD13^+$ versus $CD13^-$ cells (Figure S2K). Collectively, these analyses corroborated the fidelity of SMG and SAE organoid models in replicating the cellular heterogeneity of their respective tissues.

Human SMG organoids maintain multipotency to differentiate into SAE ciliated cells

Previous studies in mouse injury models have shown that MECs contribute to the regeneration of SMGs and SAE following injury.[8,9] To evaluate the lineage plasticity of human SMG cells, we cultured SMG-derived organoids in SAE medium. Under these conditions, the organoids exhibited increased expression of the ciliated cell marker *FOXJ1*, and immunostaining for acetylated α-tubulin confirmed the presence of ciliated cells along the apical surface, indicating a shift from mucous-producing toward ciliated cell differentiation (Figures 2J and S2L). Conversely, SAE organoids cultured in SMG medium exhibited upregulation of both *MUC5AC* and *MUC5B* expression but still preserved ciliated cell differentiation, as indicated by *FOXJ1* gene expression and cilia staining. Notably, expression of the SMG basal cell marker *KRT14* remained low in SAE organoids, suggesting that while environmental cues can influence differentiation and promote partial phenotypic shifts, the intrinsic identity of stem cells from each compartment continues to guide their lineage potential.

To further investigate the role of MECs in this cell fate transition, we explored the DEGs in MECs and identified *CD200* as an enriched surface marker compared with other SMG basal cells (Figures 2E and S2M). *CD200*, which encodes a membrane glycoprotein, has also been reported as an MEC marker in the human mammary gland.[34] To validate its specificity in labeling MECs within SMG organoids, we isolated $CD200^+$ cells and confirmed their myoepithelial identity by elevated *ACTA2* expression relative to $CD200^-$ cells (Figures 2K and S2N). We then assessed the lineage potential of $CD200^+$ and $CD200^-$ populations by culturing them in SAE-promoting conditions (Figure 2L). Both populations gave rise to organoid outgrowths, with $CD200^+$ cells displaying higher formation efficiency. However, RT-qPCR analysis showed that both populations were capable of differentiating into ciliated and mucous cell lineages, with no significant differences in marker expression (Figure S2O). These results suggest that while $CD200^+$ MECs contribute to organoid growth, SMG-derived organoids as a whole retain the capacity to differentiate into airway epithelial lineages independent of MECs.

Human SMG organoids capture differential impacts of respiratory inflammatory cytokines

Interleukin-1 beta (IL-1β) and tumor necrosis factor-alpha (TNF-α) are key pro-inflammatory cytokines that play pivotal roles in initiating and amplifying inflammatory responses within the airways (Figure 3A).[35–38] Both cytokines, produced by various immune and epithelial cells, drive the recruitment of immune cells to the site of inflammation and enhance the production of other inflammatory mediators, collectively exacerbating the inflammatory cascade. By contrast, IL-13, primarily produced during type 2 immune responses, plays a central role in promoting SAE hyperresponsiveness and mucus hypersecretion.[39,40] However, the specific impact of these inflammation-driving cytokines on SMGs remains unclear. To address this gap, we exposed SMG organoids to IL-1β, TNF-α, or IL-13 to elucidate the unique responses in SMG secretory cells.

After 7 days of treatment with inflammatory cytokines, IL-1β and IL-13 significantly reduced the percentage of $CD13^+$ cells, whereas TNF-α exhibited no specific effect (Figure 3B). Downregulation of *ANPEP*/CD13 expression has been reported in bronchial and nasal epithelium of T helper (Th)2-high asthma.[41] None of these cytokines affected the expression pattern of CD13 at the

Figure 2. Integrated scRNA-seq atlas of SMG organoids, SAE organoids, and primary airway tissue

(A) Schematic of integrated scRNA-seq datasets and corresponding cell numbers.

(B) t-Distributed stochastic neighbor embedding (tSNE) plot showing integration of SAE and SMG organoids (donor: #OHLT019) with a published human airway epithelium dataset.[21]

(C) tSNE plot displaying cluster identities from integrated scRNA-seq analysis.

(D) Left: stacked bar plot of SMG (maroon) and SAE (orange) cell contributions across clusters. Right: dot plot showing relative expression and proportion of cells expressing representative markers (three per cluster).

(E) tSNE projection of MEC score across the dataset and expression of two myoepithelial markers in the SMG basal cluster.

(F) Violin plots of MEC markers (*ACTA2*, *TAGLN*, *CNN1*, *ACTG2*, and *PCP4*), cell-cell adhesion genes (*FHOD3* and *LAMA1*), and basal cell markers (*KRT14* and *KRT5*) within the SMG basal cell cluster, split by sample.

(G) Representative immunofluorescence staining of MECs (*ACTA2*/α-SMA, red), SMG-specific mucous cells (MUC5B, green), and nuclei (DAPI, blue) in human bronchus tissues and SMG organoids (donor: #0704).

(H) Violin plots of *MUC5AC*, *MUC5B*, and *ANPEP* gene expression in SAE and SMG secretory cell clusters.

(I) Representative immunofluorescence staining of *ANPEP*/CD13 (red), MUC5B (green), and nuclei (DAPI, blue) in human bronchus SMG and SAE organoids (donor: #0704).

(J) Representative bright-field images of SAE or SMG organoids under different culture conditions (top row). Representative IHC staining of MUC5B and acetylated α-tubulin (donor: #0704).

(K) Left: representative FACS analysis of $CD200^+$ cells from SAE and SMG organoids (donor: #0523). Right: percentage of $CD200^+$ cells from SAE and SMG organoids from three independent donors. Data are shown as mean ± SEM. $^*p < 0.05$ by multiple t tests using two-stage linear step-up procedure of Benjamini, Krieger, and Yekutieli, with Q = 5%, $n = 3$.

(L) Representative bright-field time course images of $CD200^+$ and $CD200^-$ cells derived from SMG organoids (donor: #0704).

See also Figure S2.

CellPress
OPEN ACCESS

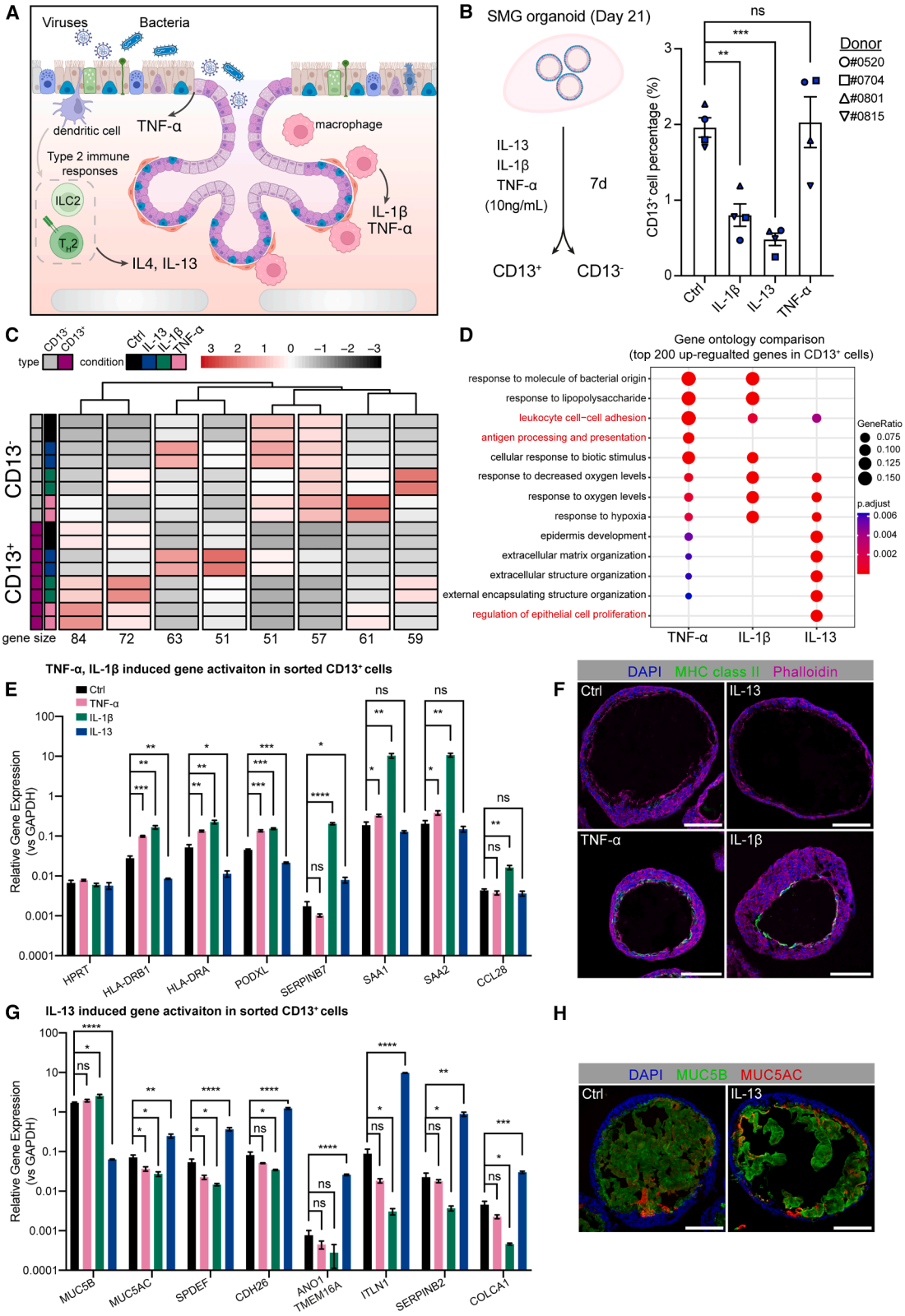

Figure 3. SMG organoids model respiratory inflammation

(A) Schematic illustrating airway inflammation, associated cell types, and cytokines.

(B) Diagram of cytokine treatments on SMG organoids (top). FACS quantification of CD13$^+$ cells from SMG organoids from multiple donors post-treatment.

(legend continued on next page)

apical surface of SMG organoids (Figure S3A). Next, we explored the impact of these cytokines on the transcriptional profiles of organoid-derived SMG secretory cells. Bulk RNA-seq of sorted $CD13^+$ and $CD13^-$ cells confirmed enrichment of SMG mucous cell markers (*MUC5B*, *BPIFB1*, *WFDC2*, *AGR2*, and *PIGR*)[42,43] and glycosylation-related pathways in $CD13^+$ cells (Figure S3B; Table S2). Subsequently, transcriptomic analysis revealed distinct cytokine-specific gene programs (Figure 3C; Table S2). IL-1β and TNF-α shared induction of innate immune and antigen presentation pathways (Figure 3D; Table S2). Further validation through RT-qPCR in SMG organoids from an independent donor demonstrated that IL-1β and TNF-α specifically induced the expression of major histocompatibility complex class II (MHC class II) genes (Figures 3E and 3F). Examination of human bronchus tissues confirmed MHC class II expression on the basolateral side of SMG secretory cells (Figure S3C). Moreover, both TNF-α and IL-1β treatments upregulated PODXL, an anti-adhesive glycoprotein involved in extracellular matrix (ECM) remodeling, which was reported to enhance interactions between antigen-presenting cells (APCs) and T cells.[44] This is in line with a recent study showing that CD4 T cells are in close proximity with human leukocyte antigen (HLA)-DR^{high} SMG epithelial cells, supporting a possible direct antigen-presenting function of SMGs.[23] Notably, IL-1β specifically induced expression of acute-phase serum amyloid A (SAA) genes: SAA1 and SAA2, which are used as biomarkers for airway inflammation and mediate local immune responses.[45–47] Furthermore, IL-1β mildly upregulated *CCL28* expression, a key component of the SMG niche chemokine previously reported by tissue spatial transcriptome profiling, highlighting its role in mediating immune cell recruitment within the glandular environment.[23]

Consistent with previous studies in 2D airway and conjunctiva epithelium cultures, IL-13 promoted cell proliferation in SMG organoid cultures (Figures 3D and S3D; Table S2).[48,49] Notably, IL-13 markedly suppressed MUC5B expression in $CD13^+$ SMG cells while enhancing MUC5AC expression (Figures 3G and 3H). This shift in mucin expression aligned with clinical observations in patients with Th2-high asthma.[50–52] Previous studies in primary human bronchial epithelial cell cultures suggested that IL-13 induces both *MUC5AC* and *MUC5B* expression through SPDEF,[53] a key transcription factor in mucous cell differentiation across different tissues.[54–56] To further explore SPDEF's role in mediating IL-13 signaling in SMGs, we conducted a CRISPR-Cas9-mediated knockout of SPDEF in SMG organoids (Figure S3E). Knocking out *SPDEF* had no impact on $CD13^+$ SMG secretory cell differentiation (Figure S3F). Interestingly, the knockout led to a marked suppression of *MUC5AC* expression without affecting MUC5B or other IL-13 targets (*CDH26*, *ANO1*, *ITLN1*, *SERPINB2*, and *COLCA1*), suggesting that SPDEF selectively mediates IL-13-driven *MUC5AC* expression in SMGs (Figure S3G).

HCoV-229E primarily targets SMG secretory cells

Respiratory virus infections are a major cause of acute COPD exacerbations.[57,58] In particular, coronavirus infections are frequently detected in the upper respiratory tract, but their specific cellular targets in human airway epithelium remain poorly defined. Prior *ex vivo* studies have produced conflicting results regarding whether human alpha-coronavirus 229E (HCoV-229E) can infect SAE.[59,60] These discrepancies may stem from variability in *ex vivo* tissue explant conditions, leaving unresolved whether HCoV-229E can effectively infect airway tissues and, if so, which cellular compartments serve as its primary targets. In this study, *ANPEP*/CD13, a known receptor for HCoV-229E,[61] was found to be predominantly expressed on the apical surface of SMGs, consistent with previous transcriptomic human lung datasets.[2] This prompted us to investigate whether $CD13^+$ SMG secretory cells serve as the primary targets for HCoV-229E infection.

SMG and SAE organoid cells were seeded on 2D transwells and cultured to confluency (Figure 4A). On day 7, culture conditions were adjusted: SMG upper chambers were filled with PBS to mimic a moist lumen, while SAE chambers were exposed to air to create an air-liquid interface. By day 21, both formed stratified layers with basal $KRT14^+$ cells and apical differentiated cells. SMG cultures were enriched for $MUC5B^+$ mucous cells, while SAE cultures predominantly featured ciliated cells.

Apical exposure to EGFP-labeled HCoV-229E (HCoV-229E-EGFP)[62] for 16 h at 33°C revealed a clear dose-dependent infection in SMG cultures with multiplicity of infection (MOI) ranging from 0 to 2, with $EGFP^+$ cells visible after 24 h and maximal cytopathic effects by 48 h (Figures 4B and S4A–S4C). Notably, HCoV-229E predominantly infected $CD13^+$ cells within SMG transwell cultures, with 30%–60% of $CD13^+$ cells infected across donors, while infection of $CD13^-$ cells remained below 1% (Figures 4C and 4D). After 14 days post-infection, EGFP signals were diminished, accompanied by a notable reduction of $CD13^+$ SMG cells within previously infected versus uninfected cultures (Figure S4D). To confirm the necessity of CD13 in viral entry, we pretreated SMG organoids with anti-CD13 antibodies prior to infection, which significantly reduced the infectivity of HCoV-229E (Figure S4E). This supports CD13 as a functional entry receptor for HCoV-229E in SMG cells. Furthermore, infection modestly increased secretion of MUC5B and MUC5AC in SMG cultures, while SAE cultures remained unaffected, further suggesting a compartment-specific infection profile (Figures S4F and S4G).

(C) Heatmap of top DEGs in $CD13^+$ or $CD13^-$ cells after cytokine treatments compared with control group by bulk RNA-seq (donor: #0704, $n = 2$).
(D) Gene ontology analysis of the top 200 upregulated genes in $CD13^+$ cells after cytokine treatments.
(E) RT-qPCR quantification of selected genes upregulated by IL-1β and TNF-α (donor: #OHLT019).
(F) Representative confocal images of human bronchus SMG organoids upon cytokine treatments (donor: #0704). The protein expressions of MHC class II (green), F-actin (phalloidin, magenta), and nuclei (DAPI, blue) are highlighted by immunofluorescence staining.
(G) RT-qPCR quantification of selected genes upregulated by IL-13 (donor: #OHLT019).
(H) Representative confocal images of SMG organoids with or without IL-13 treatment (donor: #0704), stained for MUC5B (green), MUC5AC (red), and nuclei (DAPI, blue).
Data in this figure are shown as mean ± SEM. ns, not significant; $^*p < 0.05$, $^{**}p < 0.01$, $^{***}p < 0.001$, $^{****}p < 0.0001$ by multiple t tests using two-stage linear step-up procedure of Benjamini, Krieger, and Yekutieli, with Q = 5%, $n = 3$.
See also Figure S3.

CellPress
OPEN ACCESS

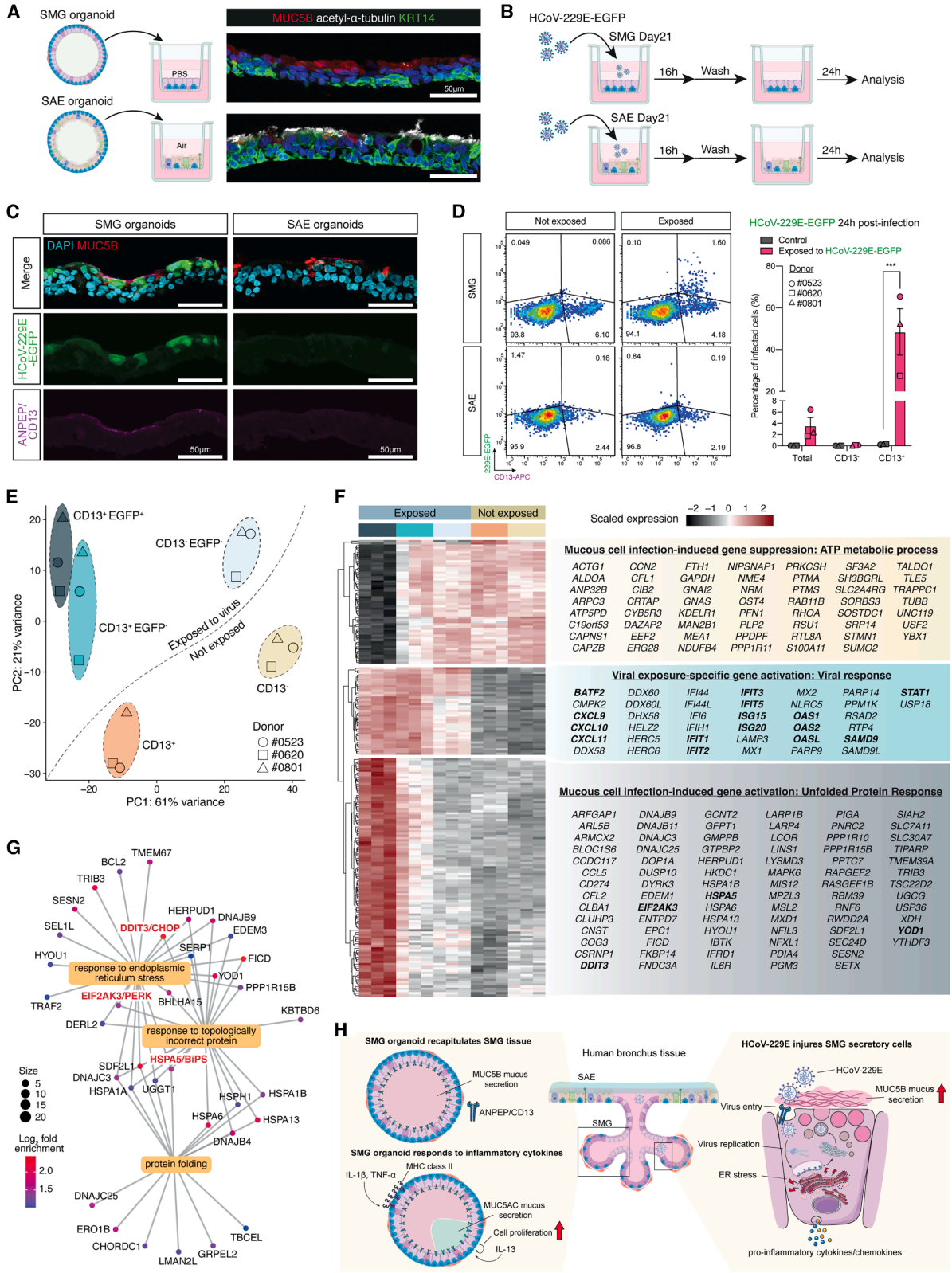

Figure 4. HCoV-229E primarily targets SMG secretory cells and causes cellular stress

(A) Left: diagram depicting transwell culture for SMG and SAE organoids. Right: representative immunofluorescence staining of SMG mucous cells (MUC5B, red), basal cells (KRT14, green), ciliated cells (acetylated α-tubulin, white), and nuclei (DAPI, blue) in transwell cultures (donor: #0704).

(legend continued on next page)

Next, to understand the transcriptional response to infection, we performed bulk RNA-seq on infected ($CD13^+EGFP^+$) SMG cells from three independent donors (Figure 4E). As expected, HCoV-229E infection unregulated interferon-responsive genes (*IFIT*, *OAS*, and the *ISG* gene family), chemokines (*CXCL9*, *CXCL10*, and *CXCL11*), and antiviral host factors (*BATF2*, *SAMD9*, and *STAT1*) (Figure 4F; Table S3). Additionally, genes involved in ATP metabolism were significantly suppressed. Interestingly, genes involved in endoplasmic reticulum (ER) stress and the unfolded protein response were significantly upregulated in infected cells. These included the central regulators (*DDIT3*/CHOP, *EIF2AK3*/PERK, and *HSPA5*/BiPS), as well as other members of heat shock protein families (Figure 4G; Table S3). RT-qPCR analysis in SMG organoids from an independent donor further confirmed the upregulation of ER stress signaling upon viral infection (Figure S4H). Additionally, infected cells exhibited increased expression of pro-inflammatory cytokines and chemokines (*IL-6*, *IL1A*, *IFNB1*, and *CXCL8*), indicating that infected cells signal the recruitment of immune cells to combat viruses. Collectively, the infected ($CD13^+EGFP^+$) SMG cells primarily contributed to the cytopathic effect upon HCoV-229E-EGFP virus infection, proposing a plausible cellular mechanism of acute exacerbation driven by ER stress.

DISCUSSION

Traditional airway models have predominantly focused on the SAE, often neglecting the complex and critical role of the SMGs. The SMG organoid model presented here enables more physiologically relevant studies of glandular components, including responses to infection and inflammation (Figure 4H). This model recapitulates key SMG features, particularly mucus-secreting cells and MECs. However, it lacks a defined serous compartment typically found in distal acinar branches.[63] Although SMG organoids can be expanded over multiple passages, serous cells are progressively lost, making early-passage organoids more suitable for studies requiring full cellular diversity, such as those on antimicrobial function and serous secretion. Given the close association between serous cells and immune components *in vivo*,[23] incorporating immune co-culture models or refining niche factor composition may provide strategies to sustain their long-term presence.

A vibrant immune environment has recently been described underlying the SMG glandular structure.[23,64] In this study, introducing IL-1β, TNF-α, and IL-13 into SMG organoid cultures revealed significant impacts on secretory cells. While previous studies have mainly focused on MHC class II expression in the SAE and lower airway,[65–67] our findings show that IL-1β and TNF-α specifically induce MHC class II expression in SMG mucous cells, consistent with observations in human bronchus tissues. Similar cytokine-driven responses have been reported in other epithelial tissues.[68,69] This highlights the potential role of SMG mucous cells in antigen presentation and immune modulation, comprising an important immune niche underlying mucosal epithelium.

HCoV-229E infection has been associated with exacerbation of COPD and asthma in epidemiological studies.[70–73] In this study, we demonstrate that HCoV-229E preferentially infects $CD13^+$ SMG cells, causing primary epithelial injury and amplifying secondary immune responses. Although airborne viruses are typically expected to infect surface epithelium, emerging evidence suggests that some respiratory viruses can directly access submucosal compartments. For example, SARS-CoV-2 variants, particularly the Delta variant, have been detected in the nasal submucosa and salivary glands,[74,75] while both human and avian influenza viruses can bind the apical surface of SMG ducts.[76] These observations imply that submucosal access may occur under specific conditions, such as impaired mucociliary clearance seen in COPD and cystic fibrosis, where thickened mucus hampers viral elimination and facilitates deeper viral penetration.[77–79] Our data indicate that HCoV-229E selectively infects SMG cells and induces ER stress and pro-inflammatory signaling, implicating this compartment in virus-driven injury. Infected SMG cells also showed elevated MUC5B and MUC5AC secretion, contributing to mucus hypersecretion and airway obstruction—hallmarks of COPD exacerbation. A previous study reported HCoV-229E infection in human airway organoids, with infection in 3D cultures requiring mechanical dissociation prior to exposure,[80] This study found higher *ANPEP*/CD13 expression in undifferentiated versus differentiated cells, resulting in higher infection rates in undifferentiated cultures. This finding contradicts the current scRNA-seq atlas of human airways and our data from sorted $CD13^+$ SMG cells. Thus, it remains crucial to examine further whether tissue-derived organoids accurately reflect the heterogeneity and functionality of their respective tissue counterparts.

Taken together, our study establishes the SMG organoid model as a new tool for investigating the complex role of SMGs in the human airway. This model effectively recapitulates key glandular cell types and, together with SAE organoids, provides a more physiologically relevant system for studying cellular responses to infections and inflammatory stimuli.

Limitations of the study

Although SAE and SMG organoids recapitulate key features of their respective tissues, integrating both compartments within

(B) Schematic of HCoV-229E infection in SMG and SAE transwell cultures.
(C) Representative immunofluorescence staining of MUC5B (red), HCoV-229E-EGFP (green), CD13 (magenta), and nuclei (DAPI, cyan) in human SMG and SAE transwell cultures infected with HCoV-229E (donor: #OHLT019).
(D) Left: representative FACS analysis of infected cultures stained with CD13-antigen-presenting cell (APC) (donor: #OHLT019). Right: quantification of infected cell types in SMG transwell cultures from three independent donors. Data are shown as mean ± SEM. ***$p < 0.001$ by two-way ANOVA using the two-stage linear step-up procedure of Benjamini, Krieger, and Yekutieli, with Q = 5%, $n = 3$.
(E) Principal-component analysis (PCA) of SMG cultures with or without HCoV-229E-EGFP infection by bulk RNA-seq ($n = 3$ donors).
(F) Heatmap of top DEGs in infected versus uninfected cells.
(G) Enrichment network plot depicting gene sets and three selected pathways by Gene oOntology analysis.
(H) Schematic summarizing the use of SMG organoids to model tissue characteristics, cytokine responses, and viral infections.
See also Figure S4.

a single culture remains technically challenging. Future studies could incorporate microfabrication approaches to enable co-culture systems that better reflect the native airway architecture. Additionally, promoting serous acini differentiation and enhancing MEC maturation may require optimized ECM compositions, biomechanical cues, or perfusion-based platforms that more closely emulate the physical and mechanical environment of the *in vivo* airway.

RESOURCE AVAILABILITY

Lead contact

Further information and requests for resources and reagents should be directed to and will be fulfilled by the lead contact, Hans Clevers (h.clevers@hubrecht.eu).

Materials availability

Sharing human organoid lines used in this study requires approval by the local institutional review board owing to hospitals' ethical regulations.

Data and code availability

- Single-cell and bulk RNA-seq data have been deposited at GEO and are publicly available as of the date of publication. This paper also analyzes existing, publicly available data. Accession numbers are listed in the key resources table.
- This paper does not report original code.
- Any additional information required to re-analyze the data reported is available from the lead contact upon request.

ACKNOWLEDGMENTS

We are grateful to all donors that agreed to participate in the study. We thank Daniel Krueger, Anko de Graaf, and the Hubrecht Imaging Centre for microscopy assistance and Reinier van der Linden, Anita Pfauth, Joost Korver, and Stefan van Elst from the Hubrecht Flow Cytometry Core Facility for flow cytometry analysis and cell sorting. We thank Gijs J.F. van Son from the Prinses Máxima Center for sequencing handling and HPC support. We thank Thanasis Margaritis, Aleksandra Balwierz, and Tito Candelli from the Máxima Single Cell Genomics Facility of the Prinses Máxima Center and Utrecht Sequencing Facility for sequencing support. We thank the National Key Research and Development Program of China (2024YFA1107702), the Strategic Priority Research Program of the Chinese Academy of Science (XDB0990102), the Shanghai Sailing Program (24YF2751500), and the Shanghai PuJiang Program (24PJA140) to L.L. C.P.C. is financially supported by the Gravitation Program "Materials Driven Regeneration," funded by the Netherlands Organization for Scientific Research (024.003.013).

AUTHOR CONTRIBUTIONS

L.L. and H.C. conceived and designed the project. L.L., C.P.C., and A.F.M.D. performed and analyzed most experiments. L.L. and C.P.C. analyzed bulk and scRNA-seq data. A.F.M.D. and T.D. assisted in writing ethical approvals for collecting human bronchus tissues from donors. M.F.M.v.O. assisted in tissue collection and pathology assessment from donor #OHLT019. N.S. performed surgery and assisted in tissue collection from donors #0523, #0620, #0704, #0801, #0815, and #0919. H.B. and J.K. performed histology experiments. L.T. and V.T. provided the HCoV-229E-EGFP virus strain, Huh-7 cell line, and experimental advice for virus handling. H.B., J.K., and S.v.d.B. provided technical support. J.H.v.E. and H.C. supervised the study and acquired funding. L.L., C.P.C., and H.C. wrote the manuscript with input from all authors.

DECLARATION OF INTERESTS

H.C. is the head of Pharma Research and Early Development at Roche and Basel and holds several patents related to organoid technology. His full disclosure can be found at https://www.uu.nl/staff/JCClevers.

STAR★METHODS

Detailed methods are provided in the online version of this paper and include the following:

SUPPLEMENTAL INFORMATION

Supplemental information can be found online at https://doi.org/10.1016/j.stem.2025.05.013.

Received: July 6, 2024
Revised: April 7, 2025
Accepted: May 23, 2025
Published: June 12, 2025

REFERENCES

1. Widdicombe, J.H. (2019). Early studies of airway submucosal glands. Am. J. Physiol. Lung Cell. Mol. Physiol. *316*, L990–L998. https://doi.org/10.1152/ajplung.00068.2019.
2. Travaglini, K.J., Nabhan, A.N., Penland, L., Sinha, R., Gillich, A., Sit, R.V., Chang, S., Conley, S.D., Mori, Y., Seita, J., et al. (2020). A molecular cell atlas of the human lung from single-cell RNA sequencing. Nature *587*, 619–625. https://doi.org/10.1038/s41586-020-2922-4.
3. Schiller, H.B., Montoro, D.T., Simon, L.M., Rawlins, E.L., Meyer, K.B., Strunz, M., Vieira Braga, F.A., Timens, W., Koppelman, G.H., Budinger, G.R.S., et al. (2019). The Human Lung Cell Atlas: A High-Resolution Reference Map of the Human Lung in Health and Disease. Am. J. Respir. Cell Mol. Biol. *61*, 31–41. https://doi.org/10.1165/rcmb.2018-0416TR.
4. Plasschaert, L.W., Žilionis, R., Choo-Wing, R., Savova, V., Knehr, J., Roma, G., Klein, A.M., and Jaffe, A.B. (2018). A single-cell atlas of the airway epithelium reveals the CFTR-rich pulmonary ionocyte. Nature *560*, 377–381. https://doi.org/10.1038/s41586-018-0394-6.
5. Fischer, A.J., Goss, K.L., Scheetz, T.E., Wohlford-Lenane, C.L., Snyder, J. M., and McCray, P.B. (2009). Differential Gene Expression in Human Conducting Airway Surface Epithelia and Submucosal Glands. Am. J. Respir. Cell Mol. Biol. *40*, 189–199. https://doi.org/10.1165/rcmb.2008-0240OC.
6. Ermund, A., Meiss, L.N., Rodriguez-Pineiro, A.M., Bähr, A., Nilsson, H.E., Trillo-Muyo, S., Ridley, C., Thornton, D.J., Wine, J.J., Hebert, H., et al. (2017). The normal trachea is cleaned by MUC5B mucin bundles from the submucosal glands coated with the MUC5AC mucin. Biochem. Biophys. Res. Commun. *492*, 331–337. https://doi.org/10.1016/j.bbrc.2017.08.113.
7. Roy, M.G., Livraghi-Butrico, A., Fletcher, A.A., Mcelwee, M.M., Evans, S. E., Boerner, R.M., Alexander, S.N., Bellinghausen, L.K., Song, A.S.,

Petrova, Y.M., et al. (2014). Muc5b is required for airway defence. Nature *505*, 412–416. https://doi.org/10.1038/nature12807.

8. Lynch, T.J., Anderson, P.J., Rotti, P.G., Tyler, S.R., Crooke, A.K., Choi, S. H., Montoro, D.T., Silverman, C.L., Shahin, W., Zhao, R., et al. (2018). Submucosal Gland Myoepithelial Cells Are Reserve Stem Cells That Can Regenerate Mouse Tracheal Epithelium. Cell Stem Cell *22*, 653–667.e5. https://doi.org/10.1016/j.stem.2018.03.017.
9. Tata, A., Kobayashi, Y., Chow, R.D., Tran, J., Desai, A., Massri, A.J., McCord, T.J., Gunn, M.D., and Tata, P.R. (2018). Myoepithelial Cells of Submucosal Glands Can Function as Reserve Stem Cells to Regenerate Airways after Injury. Cell Stem Cell *22*, 668–683.e6. https://doi.org/10.1016/j.stem.2018.03.018.
10. Restrepo, G.L., and Heard, B.E. (1963). Mucous Gland Enlargement in Chronic Bronchitis: Extent of Enlargement in the Tracheo-bronchial Tree. Thorax *18*, 334–339. https://doi.org/10.1136/thx.18.4.334.
11. Reid, L. (1960). Measurement of the Bronchial Mucous Gland Layer: A Diagnostic Yardstick in Chronic Bronchitis. Thorax *15*, 132–141. https://doi.org/10.1136/thx.15.2.132.
12. Ermund, A., Meiss, L.N., Dolan, B., Jaudas, F., Ewaldsson, L., Bähr, A., Klymiuk, N., and Hansson, G.C. (2021). Mucus threads from surface goblet cells clear particles from the airways. Respir. Res. *22*, 303. https://doi.org/10.1186/s12931-021-01898-3.
13. Ermund, A., Meiss, L.N., Dolan, B., Bähr, A., Klymiuk, N., and Hansson, G. C. (2018). The mucus bundles responsible for airway cleaning are retained in cystic fibrosis and by cholinergic stimulation. Eur. Respir. J. *52*, 1800457. https://doi.org/10.1183/13993003.00457-2018.
14. Choi, J.Y., Khansaheb, M., Joo, N.S., Krouse, M.E., Robbins, R.C., Weill, D., and Wine, J.J. (2009). Substance P stimulates human airway submucosal gland secretion mainly via a CFTR-dependent process. J. Clin. Invest. *119*, 1189–1200. https://doi.org/10.1172/JCI37284.
15. Ali, M., Maniscalco, J., and Baraniuk, J.N. (1996). Spontaneous release of submucosal gland serous and mucous cell macromolecules from human nasal explants in vitro. Am. J. Physiol. *270*, L595–L600. https://doi.org/10.1152/ajplung.1996.270.4.L595.
16. Zhou, J., Li, C., Sachs, N., Chiu, M.C., Wong, B.H.-Y., Chu, H., Poon, V. K.-M., Wang, D., Zhao, X., Wen, L., et al. (2018). Differentiated human airway organoids to assess infectivity of emerging influenza virus. Proc. Natl. Acad. Sci. USA *115*, 6822–6827. https://doi.org/10.1073/pnas.1806308115.
17. Sachs, N., Papaspyropoulos, A., Ommen, D.D.Z., Heo, I., Klay, D., Weeber, F., Huelsz-Prince, G., Iakobachvili, N., Gimano, D., de Ligt, J., et al. (2019). Long-term expanding human airway organoids for disease modeling. EMBO J. *38*, e100300. https://doi.org/10.15252/embj.2018100300.
18. Hegab, A.E., Ha, V.L., Darmawan, D.O., Gilbert, J.L., Ooi, A.T., Attiga, Y.S., Bisht, B., Nickerson, D.W., and Gomperts, B.N. (2012). Isolation and In Vitro Characterization of Basal and Submucosal Gland Duct Stem/Progenitor Cells from Human Proximal Airways. Stem Cells Transl. Med. *1*, 719–724. https://doi.org/10.5966/sctm.2012-0056.
19. Okuda, K., Chen, G., Subramani, D.B., Wolf, M., Gilmore, R.C., Kato, T., Radicioni, G., Kesimer, M., Chua, M., Dang, H., et al. (2019). Localization of Secretory Mucins MUC5AC and MUC5B in Normal/Healthy Human Airways. Am. J. Respir. Crit. Care Med. *199*, 715–727. https://doi.org/10.1164/rccm.201804-0734OC.
20. Ostedgaard, L.S., Moninger, T.O., McMenimen, J.D., Sawin, N.M., Parker, C.P., Thornell, I.M., Powers, L.S., Gansemer, N.D., Bouzek, D.C., Cook, D. P., et al. (2017). Gel-forming mucins form distinct morphologic structures in airways. Proc. Natl. Acad. Sci. USA *114*, 6842–6847. https://doi.org/10.1073/pnas.1703228114.
21. Goldfarbmuren, K.C., Jackson, N.D., Sajuthi, S.P., Dyjack, N., Li, K.S., Rios, C.L., Plender, E.G., Montgomery, M.T., Everman, J.L., Bratcher, P. E., et al. (2020). Dissecting the cellular specificity of smoking effects and reconstructing lineages in the human airway epithelium. Nat. Commun. *11*, 2485. https://doi.org/10.1038/s41467-020-16239-z.
22. Deprez, M., Zaragosi, L.-E., Truchi, M., Becavin, C., Ruiz García, S., Arguel, M.-J., Plaisant, M., Magnone, V., Lebrigand, K., Abelanet, S., et al. (2020). A Single-Cell Atlas of the Human Healthy Airways. Am. J. Respir. Crit. Care Med. *202*, 1636–1645. https://doi.org/10.1164/rccm.201911-2199OC.
23. Madissoon, E., Oliver, A.J., Kleshchevnikov, V., Wilbrey-Clark, A., Polanski, K., Richoz, N., Ribeiro Orsi, A., Mamanova, L., Bolt, L., Elmentaite, R., et al. (2023). A spatially resolved atlas of the human lung characterizes a gland-associated immune niche. Nat. Genet. *55*, 66–77. https://doi.org/10.1038/s41588-022-01243-4.
24. Dayton, T.L., Alcala, N., Moonen, L., den Hartigh, L., Geurts, V., Mangiante, L., Lap, L., Dost, A.F.M., Beumer, J., Levy, S., et al. (2023). Druggable growth dependencies and tumor evolution analysis in patient-derived organoids of neuroendocrine neoplasms from multiple body sites. Cancer Cell *41*, 2083–2099.e9. https://doi.org/10.1016/j.ccell.2023.11.007.
25. Hegab, A.E., Ha, V.L., Gilbert, J.L., Zhang, K.X., Malkoski, S.P., Chon, A. T., Darmawan, D.O., Bisht, B., Ooi, A.T., Pellegrini, M., et al. (2011). Novel Stem/Progenitor Cell Population from Murine Tracheal Submucosal Gland Ducts with Multipotent Regenerative Potential. Stem Cells *29*, 1283–1293. https://doi.org/10.1002/stem.680.
26. Sun, X., Perl, A.-K., Li, R., Bell, S.M., Sajti, E., Kalinichenko, V.V., Kalin, T. V., Misra, R.S., Deshmukh, H., Clair, G., et al. (2022). A census of the lung: CellCards from LungMAP. Dev. Cell *57*, 112–145.e2. https://doi.org/10.1016/j.devcel.2021.11.007.
27. Schmid, A., Sailland, J., Novak, L., Baumlin, N., Fregien, N., and Salathe, M. (2017). Modulation of Wnt signaling is essential for the differentiation of ciliated epithelial cells in human airways. FEBS Lett. *591*, 3493–3506. https://doi.org/10.1002/1873-3468.12851.
28. Bonser, L.R., Koh, K.D., Johansson, K., Choksi, S.P., Cheng, D., Liu, L., Sun, D.I., Zlock, L.T., Eckalbar, W.L., Finkbeiner, W.E., et al. (2021). Flow-Cytometric Analysis and Purification of Airway Epithelial-Cell Subsets. Am. J. Respir. Cell Mol. Biol. *64*, 308–317. https://doi.org/10.1165/rcmb.2020-0149MA.
29. Warner, T.F., and Azen, E.A. (1984). Proline-rich proteins are present in serous cells of submucosal glands in the respiratory tract. Am. Rev. Respir. Dis. *130*, 115–118. https://doi.org/10.1164/arrd.1984.130.1.115.
30. Liu, X., Driskell, R.R., and Engelhardt, J.F. (2004). Airway Glandular Development and Stem Cells. Curr. Top. Dev. Biol. *64*, 33–56. https://doi.org/10.1016/S0070-2153(04)64003-8.
31. Shimura, S., Sasaki, T., Sasaki, H., and Takishima, T. (1986). Contractility of isolated single submucosal gland from trachea. J. Appl. Physiol. (1985) *60*, 1237–1247. https://doi.org/10.1152/jappl.1986.60.4.1237.
32. Yu, W., Moninger, T.O., Rector, M.V., Stoltz, D.A., and Welsh, M.J. (2022). Pulmonary neuroendocrine cells sense succinate to stimulate myoepithelial cell contraction. Dev. Cell *57*, 2221–2236.e5. https://doi.org/10.1016/j.devcel.2022.08.010.
33. Anderson, P.J., Lynch, T.J., and Engelhardt, J.F. (2017). Multipotent Myoepithelial Progenitor Cells Are Born Early during Airway Submucosal Gland Development. Am. J. Respir. Cell Mol. Biol. *56*, 716–726. https://doi.org/10.1165/rcmb.2016-0304OC.
34. Goldhammer, N., Kim, J., Villadsen, R., Rønnov-Jessen, L., and Petersen, O.W. (2022). Myoepithelial progenitors as founder cells of hyperplastic human breast lesions upon PIK3CA transformation. Commun. Biol. *5*, 219. https://doi.org/10.1038/s42003-022-03161-x.
35. Mukhopadhyay, S., Hoidal, J.R., and Mukherjee, T.K. (2006). Role of TNFα in pulmonary pathophysiology. Respir. Res. *7*, 125. https://doi.org/10.1186/1465-9921-7-125.
36. Perea, L., Bottier, M., Cant, E., Richardson, H., Dicker, A.J., Shuttleworth, M., Giam, Y.H., Abo-Leyah, H., Finch, S., Huang, J.T.-J., et al. (2024). Airway IL-1β is related to disease severity and mucociliary function in bronchiectasis. Eur. Respir. J. *64*, 2301966. https://doi.org/10.1183/13993003.01966-2023.
37. Bal, S.M., Bernink, J.H., Nagasawa, M., Groot, J., Shikhagaie, M.M., Golebski, K., van Drunen, C.M., Lutter, R., Jonkers, R.E., Hombrink, P.,

et al. (2016). IL-1β, IL-4 and IL-12 control the fate of group 2 innate lymphoid cells in human airway inflammation in the lungs. Nat. Immunol. *17*, 636–645. https://doi.org/10.1038/ni.3444.

38. Chen, G., Sun, L., Kato, T., Okuda, K., Martino, M.B., Abzhanova, A., Lin, J. M., Gilmore, R.C., Batson, B.D., O'Neal, Y.K., et al. (2019). IL-1β dominates the promucin secretory cytokine profile in cystic fibrosis. J. Clin. Invest. *129*, 4433–4450. https://doi.org/10.1172/JCI125669.
39. Wills-Karp, M., Luyimbazi, J., Xu, X., Schofield, B., Neben, T.Y., Karp, C.L., and Donaldson, D.D. (1998). Interleukin-13: Central Mediator of Allergic Asthma. Science *282*, 2258–2261. https://doi.org/10.1126/science.282.5397.2258.
40. Kuperman, D.A., Huang, X., Koth, L.L., Chang, G.H., Dolganov, G.M., Zhu, Z., Elias, J.A., Sheppard, D., and Erle, D.J. (2002). Direct effects of interleukin-13 on epithelial cells cause airway hyperreactivity and mucus overproduction in asthma. Nat. Med. *8*, 885–889. https://doi.org/10.1038/nm734.
41. Coden, M.E., Loffredo, L.F., Abdala-Valencia, H., and Berdnikovs, S. (2021). Comparative Study of SARS-CoV-2, SARS-CoV-1, MERS-CoV, HCoV-229E and Influenza Host Gene Expression in Asthma: Importance of Sex, Disease Severity, and Epithelial Heterogeneity. Viruses *13*, 1081. https://doi.org/10.3390/v13061081.
42. Rose, M.C., and Voynow, J.A. (2006). Respiratory Tract Mucin Genes and Mucin Glycoproteins in Health and Disease. Physiol. Rev. *86*, 245–278. https://doi.org/10.1152/physrev.00010.2005.
43. Strous, G.J., and Dekker, J. (1992). Mucin-Type Glycoproteins. Crit. Rev. Biochem. Mol. Biol. *27*, 57–92. https://doi.org/10.3109/10409239209082559.
44. Amo, L., Díez-García, J., Tamayo-Orbegozo, E., Maruri, N., and Larrucea, S. (2022). Podocalyxin Expressed in Antigen Presenting Cells Promotes Interaction With T Cells and Alters Centrosome Translocation to the Contact Site. Front. Immunol. *13*, 835527. https://doi.org/10.3389/fimmu.2022.835527.
45. Smole, U., Gour, N., Phelan, J., Hofer, G., Köhler, C., Kratzer, B., Tauber, P.A., Xiao, X., Yao, N., Dvorak, J., et al. (2020). Serum amyloid A is a soluble pattern recognition receptor that drives type 2 immunity. Nat. Immunol. *21*, 756–765. https://doi.org/10.1038/s41590-020-0698-1.
46. Ather, J.L., Ckless, K., Martin, R., Foley, K.L., Suratt, B.T., Boyson, J.E., Fitzgerald, K.A., Flavell, R.A., Eisenbarth, S.C., and Poynter, M.E. (2011). Serum Amyloid A Activates the NLRP3 Inflammasome and Promotes Th17 Allergic Asthma in Mice. J. Immunol. *187*, 64–73. https://doi.org/10.4049/jimmunol.1100500.
47. Bozinovski, S., Hutchinson, A., Thompson, M., MacGregor, L., Black, J., Giannakis, E., Karlsson, A.-S., Silvestrini, R., Smallwood, D., Vlahos, R., et al. (2008). Serum Amyloid A Is a Biomarker of Acute Exacerbations of Chronic Obstructive Pulmonary Disease. Am. J. Respir. Crit. Care Med. *177*, 269–278. https://doi.org/10.1164/rccm.200705-678OC.
48. Tukler Henriksson, J., Coursey, T.G., Corry, D.B., De Paiva, C.S., and Pflugfelder, S.C. (2015). IL-13 Stimulates Proliferation and Expression of Mucin and Immunomodulatory Genes in Cultured Conjunctival Goblet Cells. Invest. Ophthalmol. Vis. Sci. *56*, 4186–4197. https://doi.org/10.1167/iovs.14-15496.
49. Booth, B.W., Adler, K.B., Bonner, J.C., Tournier, F., and Martin, L.D. (2001). Interleukin-13 Induces Proliferation of Human Airway Epithelial Cells In Vitro via a Mechanism Mediated by Transforming Growth Factor- α. Am. J. Respir. Cell Mol. Biol. *25*, 739–743. https://doi.org/10.1165/ajrcmb.25.6.4659.
50. Jackson, N.D., Everman, J.L., Chioccioli, M., Feriani, L., Goldfarbmuren, K.C., Sajuthi, S.P., Rios, C.L., Powell, R., Armstrong, M., Gomez, J., et al. (2020). Single-Cell and Population Transcriptomics Reveal Pan-epithelial Remodeling in Type 2-High Asthma. Cell Rep. *32*, 107872. https://doi.org/10.1016/j.celrep.2020.107872.
51. Lachowicz-Scroggins, M.E., Yuan, S., Kerr, S.C., Dunican, E.M., Yu, M., Carrington, S.D., and Fahy, J.V. (2016). Abnormalities in MUC5AC and MUC5B Protein in Airway Mucus in Asthma. Am. J. Respir. Crit. Care Med. *194*, 1296–1299. https://doi.org/10.1164/rccm.201603-0526LE.
52. Woodruff, P.G., Modrek, B., Choy, D.F., Jia, G., Abbas, A.R., Ellwanger, A., Koth, L.L., Arron, J.R., and Fahy, J.V. (2009). T-helper Type 2–driven Inflammation Defines Major Subphenotypes of Asthma. Am. J. Respir. Crit. Care Med. *180*, 388–395. https://doi.org/10.1164/rccm.200903-0392OC.
53. Koh, K.D., Siddiqui, S., Cheng, D., Bonser, L.R., Sun, D.I., Zlock, L.T., Finkbeiner, W.E., Woodruff, P.G., and Erle, D.J. (2020). Efficient RNP-directed Human Gene Targeting Reveals SPDEF Is Required for IL-13–induced Mucostasis. Am. J. Respir. Cell Mol. Biol. *62*, 373–381. https://doi.org/10.1165/rcmb.2019-0266OC.
54. Marko, C.K., Menon, B.B., Chen, G., Whitsett, J.A., Clevers, H., and Gipson, I.K. (2013). Spdef Null Mice Lack Conjunctival Goblet Cells and Provide a Model of Dry Eye. Am. J. Pathol. *183*, 35–48. https://doi.org/10.1016/j.ajpath.2013.03.017.
55. Chen, G., Korfhagen, T.R., Xu, Y., Kitzmiller, J., Wert, S.E., Maeda, Y., Gregorieff, A., Clevers, H., and Whitsett, J.A. (2009). SPDEF is required for mouse pulmonary goblet cell differentiation and regulates a network of genes associated with mucus production. J. Clin. Invest. *119*, 2914–2924. https://doi.org/10.1172/JCI39731.
56. Gregorieff, A., Stange, D.E., Kujala, P., Begthel, H., van den Born, M., Korving, J., Peters, P.J., and Clevers, H. (2009). The Ets-Domain Transcription Factor Spdef Promotes Maturation of Goblet and Paneth Cells in the Intestinal Epithelium. Gastroenterology *137*, 1333–1345.e1. https://doi.org/10.1053/j.gastro.2009.06.044.
57. Mohan, A., Chandra, S., Agarwal, D., Guleria, R., Broor, S., Gaur, B., and Pandey, R.M. (2010). Prevalence of viral infection detected by PCR and RT-PCR in patients with acute exacerbation of COPD: A systematic review. Respirology *15*, 536–542. https://doi.org/10.1111/j.1440-1843.2010.01722.x.
58. Varkey, J.B., and Varkey, B. (2008). Viral infections in patients with chronic obstructive pulmonary disease. Curr. Opin. Pulm. Med. *14*, 89–94. https://doi.org/10.1097/MCP.0b013e3282f4a99f.
59. Chan, R.W.Y., Chan, M.C.W., Agnihothram, S., Chan, L.L.Y., Kuok, D.I.T., Fong, J.H.M., Guan, Y., Poon, L.L.M., Baric, R.S., Nicholls, J.M., et al. (2013). Tropism of and Innate Immune Responses to the Novel Human Betacoronavirus Lineage C Virus in Human Ex Vivo Respiratory Organ Cultures. J. Virol. *87*, 6604–6614. https://doi.org/10.1128/JVI.00009-13.
60. Wang, G., Deering, C., Macke, M., Shao, J., Burns, R., Blau, D.M., Holmes, K.V., Davidson, B.L., Perlman, S., and McCray, P.B. (2000). Human Coronavirus 229E Infects Polarized Airway Epithelia from the Apical Surface. J. Virol. *74*, 9234–9239. https://doi.org/10.1128/JVI.74.19.9234-9239.2000.
61. Yeager, C.L., Ashmun, R.A., Williams, R.K., Cardellichio, C.B., Shapiro, L. H., Look, A.T., and Holmes, K.V. (1992). Human aminopeptidase N is a receptor for human coronavirus 229E. Nature *357*, 420–422. https://doi.org/10.1038/357420a0.
62. Cervantes-Barragan, L., Züst, R., Maier, R., Sierro, S., Janda, J., Levy, F., Speiser, D., Romero, P., Rohrlich, P.-S., Ludewig, B., et al. (2010). Dendritic Cell-Specific Antigen Delivery by Coronavirus Vaccine Vectors Induces Long-Lasting Protective Antiviral and Antitumor Immunity. mBio *1*, e00171-10. https://doi.org/10.1128/mBio.00171-10.
63. Meyrick, B., Sturgess, J.M., and Reid, L. (1969). A reconstruction of the duct system and secretory tubules of the human bronchial submucosal gland. Thorax *24*, 729–736. https://doi.org/10.1136/thx.24.6.729.
64. Hewitt, R.J., and Lloyd, C.M. (2021). Regulation of immune responses by the airway epithelial cell landscape. Nat. Rev. Immunol. *21*, 347–362. https://doi.org/10.1038/s41577-020-00477-9.
65. Shenoy, A.T., Lyon De Ana, C., Arafa, E.I., Salwig, I., Barker, K.A., Korkmaz, F.T., Ramanujan, A., Etesami, N.S., Soucy, A.M., Martin, I.M. C., et al. (2021). Antigen presentation by lung epithelial cells directs CD4+ TRM cell function and regulates barrier immunity. Nat. Commun. *12*, 5834. https://doi.org/10.1038/s41467-021-26045-w.
66. Vignola, A.M., Campbell, A.M., Chanez, P., Bousquet, J., Paul-Lacoste, P., Michel, F.B., and Godard, P. (1993). HLA-DR and ICAM-1 Expression

on Bronchial Epithelial Cells in Asthma and Chronic Bronchitis. Am. Rev. Respir. Dis. *148*, 689–694. https://doi.org/10.1164/ajrccm/148.3.689.

67. Glanville, A.R., Tazelaar, H.D., Theodore, J., Imoto, E., Rouse, R.V., Baldwin, J.C., and Robin, E.D. (1989). The Distribution of MHC Class I and II Antigens on Bronchial Epithelium. Am. Rev. Respir. Dis. *139*, 330–334. https://doi.org/10.1164/ajrccm/139.2.330.
68. Keller, C.W., Fokken, C., Turville, S.G., Lünemann, A., Schmidt, J., Münz, C., and Lünemann, J.D. (2011). TNF-α Induces Macroautophagy and Regulates MHC Class II Expression in Human Skeletal Muscle Cells. J. Biol. Chem. *286*, 3970–3980. https://doi.org/10.1074/jbc.M110.159392.
69. von Burg, N., Chappaz, S., Baerenwaldt, A., Horvath, E., Bose Dasgupta, S., Ashok, D., Pieters, J., Tacchini-Cottier, F., Rolink, A., Acha-Orbea, H., et al. (2014). Activated group 3 innate lymphoid cells promote T-cell–mediated immune responses. Proc. Natl. Acad. Sci. USA *111*, 12835–12840. https://doi.org/10.1073/pnas.1406908111.
70. Seemungal, T., Harper-Owen, R., Bhowmik, A., Moric, I., Sanderson, G., Message, S., Maccallum, P., Meade, T.W., Jeffries, D.J., Johnston, S.L., et al. (2001). Respiratory Viruses, Symptoms, and Inflammatory Markers in Acute Exacerbations and Stable Chronic Obstructive Pulmonary Disease. Am. J. Respir. Crit. Care Med. *164*, 1618–1623. https://doi.org/10.1164/ajrccm.164.9.2105011.
71. Gorse, G.J., O'Connor, T.Z., Hall, S.L., Vitale, J.N., and Nichol, K.L. (2009). Human Coronavirus and Acute Respiratory Illness in Older Adults with Chronic Obstructive Pulmonary Disease. J. Infect. Dis. *199*, 847–857. https://doi.org/10.1086/597122.
72. Falsey, A.R., Walsh, E.E., and Hayden, F.G. (2002). Rhinovirus and Coronavirus Infection–Associated Hospitalizations among Older Adults. J. Infect. Dis. *185*, 1338–1341. https://doi.org/10.1086/339881.
73. Nicholson, K.G., Kent, J., and Ireland, D.C. (1993). Respiratory viruses and exacerbations of asthma in adults. BMJ *307*, 982–986. https://doi.org/10.1136/bmj.307.6910.982.
74. Chen, M., Pekosz, A., Villano, J.S., Shen, W., Zhou, R., Kulaga, H., Li, Z., Smith, A., Gurung, A., Beck, S.E., et al. (2024). Evolution of nasal and olfactory infection characteristics of SARS-CoV-2 variants. J. Clin. Invest. *134*, e174439. https://doi.org/10.1172/JCI174439.
75. Huang, N., Pérez, P., Kato, T., Mikami, Y., Okuda, K., Gilmore, R.C., Conde, C.D., Gasmi, B., Stein, S., Beach, M., et al. (2021). SARS-CoV-2 infection of the oral cavity and saliva. Nat. Med. *27*, 892–903. https://doi.org/10.1038/s41591-021-01296-8.
76. van Riel, D., den Bakker, M.A., Leijten, L.M.E., Chutinimitkul, S., Munster, V.J., de Wit, E., Rimmelzwaan, G.F., Fouchier, R.A.M., Osterhaus, A.D.M. E., and Kuiken, T. (2010). Seasonal and Pandemic Human Influenza Viruses Attach Better to Human Upper Respiratory Tract Epithelium than Avian Influenza Viruses. Am. J. Pathol. *176*, 1614–1618. https://doi.org/10.2353/ajpath.2010.090949.
77. Hill, D.B., Long, R.F., Kissner, W.J., Atieh, E., Garbarine, I.C., Markovetz, M.R., Fontana, N.C., Christy, M., Habibpour, M., Tarran, R., et al. (2018). Pathological mucus and impaired mucus clearance in cystic fibrosis patients result from increased concentration, not altered pH. Eur. Respir. J. *52*, 1801297. https://doi.org/10.1183/13993003.01297-2018.
78. Livraghi, A., and Randell, S.H. (2007). Cystic Fibrosis and Other Respiratory Diseases of Impaired Mucus Clearance. Toxicol. Pathol. *35*, 116–129. https://doi.org/10.1080/01926230601060025.
79. Smaldone, G.C., Foster, W.M., O'Riordan, T.G., Messina, M.S., Perry, R. J., and Langenback, E.G. (1993). Regional Impairment of Mucociliary Clearance in Chronic Obstructive Pulmonary Disease. Chest *103*, 1390–1396. https://doi.org/10.1378/chest.103.5.1390.
80. Li, P., Wang, Y., Lamers, M.M., Lavrijsen, M., Iriondo, C., de Vries, A.C., Rottier, R.J., Peppelenbosch, M.P., Haagmans, B.L., and Pan, Q. (2022). Recapitulating infection, thermal sensitivity and antiviral treatment of seasonal coronaviruses in human airway organoids. EBioMedicine *81*, 104132. https://doi.org/10.1016/j.ebiom.2022.104132.
81. Hao, Y., Stuart, T., Kowalski, M.H., Choudhary, S., Hoffman, P., Hartman, A., Srivastava, A., Molla, G., Madad, S., Fernandez-Granda, C., et al. (2024). Dictionary learning for integrative, multimodal and scalable single-cell analysis. Nat. Biotechnol. *42*, 293–304. https://doi.org/10.1038/s41587-023-01767-y.
82. Wickham, H. (2016). ggplot2 (Springer International Publishing). https://doi.org/10.1007/978-3-319-24277-4.
83. Love, M.I., Huber, W., and Anders, S. (2014). Moderated estimation of fold change and dispersion for RNA-seq data with DESeq2. Genome Biol. *15*, 550. https://doi.org/10.1186/s13059-014-0550-8.
84. Kolde, R. (2018). pheatmap: Pretty Heatmaps. R package version 1.0.12. https://github.com/raivokolde/pheatmap.
85. Yu, G., Wang, L.-G., Han, Y., and He, Q.-Y. (2012). clusterProfiler: an R Package for Comparing Biological Themes Among Gene Clusters. OMICS *16*, 284–287. https://doi.org/10.1089/omi.2011.0118.
86. Wu, T., Hu, E., Xu, S., Chen, M., Guo, P., Dai, Z., Feng, T., Zhou, L., Tang, W., Zhan, L., et al. (2021). clusterProfiler 4.0: A universal enrichment tool for interpreting omics data. Innovation (Camb) *2*, 100141. https://doi.org/10.1016/j.xinn.2021.100141.
87. Lin, L., DeMartino, J., Wang, D., van Son, G.J.F., van der Linden, R., Begthel, H., Korving, J., Andersson-Rolf, A., van den Brink, S., Lopez-Iglesias, C., et al. (2023). Unbiased transcription factor CRISPR screen identifies ZNF800 as master repressor of enteroendocrine differentiation. Science *382*, 451–458. https://doi.org/10.1126/science.adi2246.
88. Fujii, M., Matano, M., Nanki, K., and Sato, T. (2015). Efficient genetic engineering of human intestinal organoids using electroporation. Nat. Protoc. *10*, 1474–1485. https://doi.org/10.1038/nprot.2015.088.
89. Stuart, T., Butler, A., Hoffman, P., Hafemeister, C., Papalexi, E., Mauck, W. M., Hao, Y., Stoeckius, M., Smibert, P., and Satija, R. (2019). Comprehensive Integration of Single-Cell Data. Cell *177*, 1888–1902. e21. https://doi.org/10.1016/j.cell.2019.05.031.
90. Blackburn, J.B., Li, N.F., Bartlett, N.W., and Richmond, B.W. (2023). An update in club cell biology and its potential relevance to chronic obstructive pulmonary disease. Am. J. Physiol. Lung Cell. Mol. Physiol. *324*, L652–L665. https://doi.org/10.1152/ajplung.00192.2022.
91. Tirosh, I., Izar, B., Prakadan, S.M., Wadsworth, M.H., Treacy, D., Trombetta, J.J., Rotem, A., Rodman, C., Lian, C., Murphy, G., et al. (2016). Dissecting the multicellular ecosystem of metastatic melanoma by single-cell RNA-seq. Science *352*, 189–196. https://doi.org/10.1126/science.aad0501.
92. Danopoulos, S., Bhattacharya, S., Mariani, T.J., and Al Alam, D. (2020). Transcriptional characterisation of human lung cells identifies novel mesenchymal lineage markers. Eur. Respir. J. *55*, 1900746. https://doi.org/10.1183/13993003.00746-2019.

STAR★METHODS

KEY RESOURCES TABLE

REAGENT or RESOURCE	SOURCE	IDENTIFIER
Antibodies		
Anti-MUC5B Antibody	Atlas Antibodies	Cat#HPA008246; RRID:AB_1854203
MUC5AC Monoclonal Antibody (45M1)	Thermo Fisher Scientific	Cat#MA5-12178; RRID:AB_10978001
Acetylated alpha Tubulin Antibody (6–11B-1)	Santa Cruz	Cat#sc-23950; RRID:AB_628409
CD13 Monoclonal antibody	ProteinTech	Cat#66211-1-Ig; RRID:AB_2881602
Ultra-LEAF(TM) Purified anti-human CD13	BioLegend	Cat#301723; RRID: AB_2728236
Anti-CD13 Antibody	Antibodies.com	Cat#A86409; RRID: AB_2749503
APC anti-human CD13 Antibody	BioLegend	Cat#301706; RRID:AB_314182
APC anti-human CD200 (OX2) Antibody	BioLegend	Cat# 399807; RRID:AB_2904425
Alpha-Smooth Muscle Actin Monoclonal Antibody (1A4 (asm-1))	Thermo Fisher Scientific	Cat#MA5-11547; RRID:AB_10979529
Mouse Anti-Human HLA-DR, DP, DQ	BD Biosciences	Cat#555556; RRID:AB_395938
Mouse anti-Ki67 Antigen, clone MM1 (monoclonal)	MONOSAN	Cat#MONX10283; RRID:AB_1833494
Keratin 14 Polyclonal Chicken Antibody, Purified	BioLegend	Cat#906004; RRID:AB_2616962
Goat anti-Rabbit IgG (H+L) Secondary Antibody, HRP	Thermo Fisher Scientific	Cat#32460; RRID:AB_1185567
Rabbit Anti-Mouse Immunoglobulins/HRP (Ig Fraction)	Agilent	Cat#P0161; RRID:AB_2687969
Alexa Fluor 488 donkey anti-rabbit	Thermo Fisher Scientific	Cat#A21206; RRID: AB_2535792
Alexa Fluor 488 donkey anti-chicken	Thermo Fisher Scientific	Cat#A78948; RRID: AB_2921070
Alexa Fluor 568 donkey anti-mouse	Thermo Fisher Scientific	Cat#A10037; RRID: AB_2534013
Alexa Fluor 568 donkey anti-rabbit	Thermo Fisher Scientific	Cat#A10042; RRID: AB_2534017
Alexa Fluor 647 donkey anti-rabbit	Thermo Fisher Scientific	Cat#A-31573; RRID: AB_2536183
Phalloidin–Atto 647N	Sigma-Aldrich	Cat#65906
EnVision+ Single Reagent (HRP. Mouse)	Agilent	Cat#K400111-2
BrightVision+ Anti-Rabbit IgG (H+L) (Poly-HRP)	Avantor	Cat#DPVR110HRP
Chemicals and Recombinant Proteins		
Advanced DMEM/F-12	Thermo Fisher Scientific	Cat#12634028
DMEM, high glucose, GlutaMAX™ Supplement, HEPES	Thermo Fisher Scientific	Cat#10564011
Opti-MEM™ I Reduced Serum Medium	Thermo Fisher Scientific	Cat#11058021
Penicillin-Streptomycin (10,000 U/mL)	Thermo Fisher Scientific	Cat#15140122
HEPES (1M)	Thermo Fisher Scientific	Cat#15630056
GlutaMAX™ Supplement	Thermo Fisher Scientific	Cat#35050038
Primocin (50mg/mL)	InvivoGen	Cat#ant-pm-1
B-27™ Supplement (50X), minus vitamin A	Thermo Fisher Scientific	Cat#12587010
Cultrex Basement Membrane Extract (BME), Growth Factor Reduced, Type 2	R&D Systems, Bio-Techne	3533-001-02
TrypLE™ Express Enzyme (1X), phenol red	Thermo Fisher Scientific	Cat#12605010
Pronase	Sigma-Aldrich	Cat#10165921001
DNase I	Sigma-Aldrich	Cat#10104159001
Collagenase from *Clostridium histolyticum*	Sigma-Aldrich	Cat#C9407
Red Blood Cell Lysis Buffer	Sigma-Aldrich	Cat#11814389001
Noggin-fc fusion protein conditioned medium	U-PROTEIN EXPRESS BV	Cat#N002 - 100 ml
Animal-Free Recombinant Human FGF-10	Peprotech	Cat#AF-100-26
Animal-Free Recombinant Human KGF (FGF-7)	Peprotech	Cat#AF-100-19
Recombinant Human IL-13	Peprotech	Cat#200-13
Recombinant Human TNF-α	Peprotech	Cat#300-01A
Recombinant Human IL-1β	Peprotech	Cat#200-01B

(*Continued on next page*)

Continued

REAGENT or RESOURCE	SOURCE	IDENTIFIER
A83-01	Tocris	Cat#2939
SB202190	Sigma-Aldrich	Cat# S7067
N-Acetyl-L-cysteine	Sigma-Aldrich	Cat#A9165
Nicotinamide (1M)	Sigma-Aldrich	Cat#N0636
Lenti-X™ Concentrator	Takara Bio	Cat#631232
Recombinant RNasin® RNase Inhibitor, 10,000 U	Promega	Cat#N2515
GoScript™ Reverse Transcriptase kit	Promega	Cat#A5000
Oligo(dT) 15 Primer, 500ug/ml 20ug	Promega	Cat#C1101
Random Primer, 500ug/ml 20ug	Promega	Cat#C1181
BbsI-HF	NEB	Cat#R3539S
Y-27632 dihydrochloride	Abmole Bioscience	Cat#M1817
iQ™ SYBR® Green Supermix	BioRad	Cat#1708887
DAPI, 4′,6-Diamidine-2′-phenylindole dihydrochloride	Sigma-Aldrich	Cat#10236276001
DRAQ5	Biostatus	Cat#DR05500
TRIzol Reagent	Thermo Fisher Scientific	Cat#15596026
Tissue Freezing Medium	Leica Biosystems	Cat#14020108926
VECTASHIELD® Antifade Mounting Medium	VectorLabs	Cat#H-1000-10
Nitrocellulose Membrane	Bio-Rad	Cat#1620115
Critical Commercial Assays		
NucleoSpin RNA, Mini kit for RNA purification	MACHEREY-NAGEL	Cat#740955.50
Miniprep DNA isolation kit	Thermo Fisher Scientific	Cat#K210003
NucleoBond Xtra Midi Plus kit for transfection-grade plasmid DNA	MACHEREY-NAGEL	Cat#740412.50
Quick-DNA Microprep Kit	Zymo Research	Cat#D3021
Lenti-X™ qRT-PCR Titration Kit	Takara Bio	Cat#631235
Amersham ECL Prime Western Blotting Detection Reagent	Cytiva	Cat#RPN2232
Deposited Data		
scRNA-seq profiling of human SMG and SAE organoids	This paper	GEO: GSE271084
Bulk RNA-seq profiling of human SMG organoids upon cytokine treatments	This paper	GEO: GSE271148
Bulk RNA-seq profiling of human SMG organoids upon virus infection	This paper	GEO: GSE271264
Processed human airway single-cell atlas	Goldfarbmuren et al.[21]	GEO: GSE134174
Recombinant DNA		
sgBbsI (p2Tol-U6-2xBbsI-sgRNA-HygR)	Addgene	Cat#71485
spCas9-BlastR (pCBhCas9-BlastR)	Addgene	Cat#71489
Software and Algorithms		
FlowJo software (v.10.4)	FlowJo	https://www.flowjo.com
Fiji	NIH, Fiji developers	https://imagej.net/Fiji
Prism (v.8.2.0)	GraphPad	https://www.graphpad.com/scientific-software/prism/
Rstudio	Rstudio	https://rstudio.com/
R (v.4.3.3)	R Core	https://www.r-project.org/
Seurat (v.5.1.0)	Hao et al.[81]	https://satijalab.org/seurat/index.html
ggplot2 (v.3.5.1)	Wickham[82]	https://ggplot2.tidyverse.org/index.html
DESeq2 (v.1.36.0)	Love et al.[83]	https://github.com/mikelove/DESeq2
pheatmap (v.1.0.12)	Kolde, R.[84]	https://cran.r-project.org/web/packages/pheatmap/index.html

(*Continued on next page*)

Continued

REAGENT or RESOURCE	SOURCE	IDENTIFIER
clusterProfiler (v.4.7.1.002)	Yu et al.[85]	https://yulab-smu.top/biomedical-knowledge-mining-book/
Enrichplot (v.1.18.3)	Wu et al.[86] and Yu et al.[85]	https://doi.org/10.1016/j.xinn.2021.100141
Biorender	Biorender	http://www.biorender.com
Experimental Models: organoid lines and cell lines		
Donor: #OHLT019		HUB
Donor: #0523		Diakonessenhuis Utrecht-Hubrecht
Donor: #0620		Diakonessenhuis Utrecht-Hubrecht
Donor: #0703		Diakonessenhuis Utrecht-Hubrecht
Donor: #0801		Diakonessenhuis Utrecht-Hubrecht
Donor: #0815		Diakonessenhuis Utrecht-Hubrecht
Donor: #0919		Diakonessenhuis Utrecht-Hubrecht
Huh-7	Kindly provided by Dr. Volker Thiel (University of Bern, Switzerland)	N/A
Experimental Models: virus strains		
HCoV-229E-EGFP	Kindly provided by Dr. Volker Thiel (University of Bern, Switzerland), Cervantes-Barragan et al.[62]	https://doi.org/10.1128/mBio.00171-10
Oligonucleotides		
qPCR primers	This paper, and Table S4 Oligo collection	N/A
Viral titer primers	This paper, and Table S4 Oligo collection	N/A

EXPERIMENTAL MODEL AND STUDY PARTICIPANT DETAILS

Human samples

Human bronchus samples were obtained as healthy adjacent tissues from tumor resections at the St Antonius Hospital Utrecht (#OHLT019), or at the Diakonessen Hospital Utrecht (#0523, #0620, #0704, #0801, #0815, and #0919) (Utrecht, the Netherlands). The study was approved by the ethical committee and was in accordance with the Declaration of Helsinki and according to Dutch law. This study is compliant with all relevant ethical regulations regarding research involving human participants. As patient samples were anonymized, sex, gender, age, race and other information were not recorded and hence are not available.

Viruses

HCoV-229E containing endogenously tagged EGFP protein by replacing accessory gene 4 (HCoV-229E-EGFP) was a kind gift from Volker Thiel (University of Bern, Switzerland).[62] Biosafety level 2 (BSL-2) infections were conducted at the Hubrecht Institute following Dutch regulations.

METHOD DETAILS

Organoid culture

Bronchus samples with cartilaginous rings were dissected using fine-tip surgical scissors to expose the surface airway and resuspended in 1.5 mg/mL Pronase in digestion buffer, which contained Advanced Dulbecco's modified Eagle's medium (DMEM)/F12 (Thermo Fisher Scientific) supplemented with Y-27632 dihydrochloride (10 μM, Abmole Bioscience), Primocin (100 μg/mL, InvivoGen), and 10 U/mL DNase I (Sigma-Aldrich), at 4°C for 2 hours with gentle nutation. The tube with bronchus samples was then placed at 37°C for 30 minutes, and the tissue suspension was vigorously pipetted up and down using a P1000 pipette every 5 minutes. The detached SAE cells were collected in a separate tube, washed, and pelleted at 300xg for 3 minutes.

The remaining bronchus tissues were then placed in a petri dish and dissected with fine-tip surgical scissors into tissue pieces $\leq$ 5 mm^3. Pre-warmed Collagenase (Sigma-Aldrich) diluted in digestion buffer was added to the tissue pieces to a final concentration of 1 mg/mL, followed by incubation at 37°C for 15 minutes. The tissue suspension was vigorously pipetted up and down using a P1000 pipette every 5 minutes. The cell suspension containing the remaining detached SAE cell sheets was collected, washed, and combined with the previously collected SAE samples.

The tissue suspension was again placed in a petri dish and dissected with a surgical knife and micro scissors to remove the cartilaginous rings. The SMGs entangled with connective tissues were cut and collected into fresh digestion medium with 1 mg/mL Collagenase (Sigma-Aldrich) at 37°C for 15 minutes. The tissue suspension was vigorously pipetted up and down using a P1000 pipette every 5 minutes until the SMGs were released from connective tissues. The resulting cell suspension containing SMGs was collected, washed, and pelleted at 300xg for 3 minutes. If the cell pellets of SMGs and SAE presented red blood cells, they were resuspended in 1 mL of Red Blood Cell Lysis Buffer (Sigma-Aldrich) and incubated at room temperature for 5 minutes. The SMG and SAE cell pellets were washed twice with digestion buffer and seeded separately in Cultrex Basement Membrane Extract (BME, Growth Factor Reduced, Type 2, R&D Systems) in cell suspension plate (Corning).

The compositions of culture media for human SMG and SAE organoids are listed in Figure 1B. The concentrations are: Noggin conditioned medium (1%, U-Protein Express), n-Acetyl Cysteine (1.25 mM, Sigma-Aldrich), Nicotinamide (5 mM, Sigma-Aldrich), human FGF-10 (50 ng/mL, PeproTech), human FGF-7 (25 ng/mL, PeproTech), A83-01 (500 nM, Tocris), p38 inhibitor SB202190 (1 μM, Sigma-Aldrich), supplemented in basic culture medium consisting of Advanced Dulbecco's modified Eagle's medium (DMEM)/F12 with B27 (minus vitamin A, 1%, Thermo Fisher Scientific), Glutamax (1%, Thermo Fisher Scientific), HEPES (1%, Thermo Fisher Scientific), and penicillin/streptomycin (1%, Thermo Fisher Scientific). Rho kinase inhibitor Y-27632 dihydrochloride (10 μM, Abmole Bioscience) and Primocin (100 μg/mL, InvivoGen) were added upon passaging.

SMG and SAE organoids were split every 21-28 days and the medium was refreshed every three days. For passaging, organoids were removed from the BME (R&D Systems) and digested with prewarmed TrypLE (Thermo Fisher Scientific) at 37°C for 2-3 minutes. The organoids were vigorously pipetted up and down using glass Pasteur pipettes until they were mostly dissociated into small cell clumps (<10 cells). The digested cell suspension was then washed twice with AdDMEM/F12 (Thermo Fisher Scientific) and replated in fresh BME (R&D Systems).

Cytokine treatments

Stock solutions for cytokines were prepared according to manufacturer's recommendation. Recombinant human IL-13 (Peprotech), Recombinant human TNF-α (Peprotech), and Recombinant human IL-1β (Peprotech) were added to organoid cultures to a final concentration of 10 ng/mL. The medium was replenished every 2 days until Day 7. Cells were then harvested for further analysis.

HCoV-229E-EGFP propagation and titration quantification

Huh-7 cells, kindly provided by Dr. Volker Thiel (University of Bern, Switzerland), were cultured in DMEM with high glucose and GlutaMAX Supplement (Thermo Fisher Scientific), containing 10% FBS and 1% Penicillin/Streptomycin. The cells were maintained at 37°C with 5% CO2. On day 0, Huh-7 cells were inoculated with HCoV-229E-EGFP virus and incubated at 33°C for 24 hours post-infection. After incubation, cells were washed with PBS and further cultured in fresh medium. Cells were monitored daily under a light microscope until strong cytopathic effects became visible on day 4. Supernatant was harvested daily, centrifuged for 5 minutes at 300xg at 4°C, filtered through a 45 μm pore size polyethersulfone membrane filter, and stored at 4°C. Once all batches of supernatants were collected, they were combined and concentrated using Lenti-X Concentrator (Takara Bio) according to the manufacturer's protocol. The concentrated virus was resuspended in 1/100th of the original volume using AdDMEM/F12 (Thermo Fisher Scientific), aliquoted into 100 μL/tube, and stored at -80°C.

For virus titration, genomic RNA from HCoV-229E-EGFP virus particles was isolated from concentrated aliquots using the Nucleospin RNA Virus Kit (Macherey-Nagel) and treated with DNase I (Thermo Fisher Scientific). Quantitation was performed in a qRT-PCR reaction using primers targeting the nucleocapsid (N) encoding gene locus (Table S4), following the protocol of the Lenti-X qRT-PCR Titration Kit (Takara Bio), yielding an approximate concentration of 1*10∧6 virus particles per μL of the concentrated virus mixture. To achieve an optimal infection titration with a multiplicity of infection (MOI) smaller than 1, a series of test infection experiments were performed on SMG transwell cultures with serial dilutions of the concentrated virus mixture. All HCoV-229E-EGFP infection experiments were conducted at 33°C.

CRISPR/Cas9-mediated knockout in SMG organoids

For generating the SPDEF$^{-/-}$ knockout organoid line, we dissociated the SMG organoids into single cells and filtered them through a 35 μm nylon mesh cell strainer (Falcon) prior to electroporation. CRISPR/Cas9-mediated gene knockout in organoids was performed as previously described.[87] sgRNA targeting *SPDEF* was designed and cloned into the vector sgBbsI (p2Tol-U6-2xBbsI-sgRNA-HygR) (Addgene #71485) at the BbsI restriction enzyme cutting site. Together with p2T-CAG-SpCas9-BlastR (Addgene #107190), a 10 μg plasmid mixture was introduced into the digested organoid cells in Opti-MEM (Thermo Fisher Scientific) using the NEPA electroporation system (NEPAGENE) as previously described, with the poring pulse voltage adjusted to 150 V.[88] Organoid clones derived from single-cell expansion were manually picked and expanded for genotyping. The gRNA sequences and genotyping primers are listed in Table S4. The sgBbsI (p2Tol-U6-2xBbsI-sgRNA-HygR) vector was a gift from Richard Sherwood (Addgene plasmid # 71485; http://n2t.net/addgene:71485; RRID:Addgene_71485). The p2T-CAG-SpCas9-BlastR vector was a gift from Richard Sherwood (Addgene plasmid # 107190; http://n2t.net/addgene:107190; RRID:Addgene_107190).

RNA extraction and real-time PCR analysis

For organoids cultured in 3D, organoid cultures subjected to different treatments were removed from BME (R&D Systems) and washed with DPBS (Thermo Fisher Scientific). RNA purification was performed using the NucleoSpin RNA Mini kit (MACHEREY-NAGEL),

following the manufacturer's protocol. DNase-treated RNA was resuspended in nuclease-free water and quantified using a Nanodrop spectrophotometer (Thermo Fisher Scientific). For each reverse transcription reaction, 1-2 μg of DNase-treated RNA was used with Oligo(dT)15 Primer (Promega) or Random Primer (Promega) and the GoScript™ Reverse Transcriptase kit (Promega). The cDNA was subsequently subjected to qPCR using iQ™ SYBR® Green supermix (Bio-Rad) in a CFX Connect™ Real-Time PCR machine (Bio-Rad). Gene expression profiling was performed using gene-specific qPCR primers. The Ct readouts of each gene were first normalized against the housekeeping gene GAPDH (ΔCt), and the relative expression levels of individual genes under experimental conditions versus control conditions were calculated using the 2-ΔΔCt method. All qPCR primers are listed in Table S4.

For organoids subjected to CD13 staining or virus infection, sorted cells were collected in Buffer RA1 from the NucleoSpin RNA Kit (Macherey-Nagel) and then subjected to RNA purification, followed by cDNA synthesis. For each reverse transcription reaction, 4000-8000 cells per condition were sorted per replicate. Equivalent cell numbers from different conditions were used for each experiment to ensure consistency.

Flow cytometry

Organoids were removed from BME (R&D Systems), digested with TrypLE (Thermo Fisher Scientific) for 5 minutes into single cells using glass Pasteur pipettes, washed with ice-cold AdDMEM/F12 (Thermo Fisher Scientific), and filtered into FACS tubes through a cell strainer (Falcon). Prior to FACS, cells were stained with DAPI (Sigma-Aldrich) to identify live cells.

For cells subjected to RNA isolation, Buffer RA1 from the NucleoSpin RNA Kit (Macherey-Nagel) was used as the collection buffer. For cells subjected to flow cytometry analysis, we used an analysis buffer consisting of 5 mM EDTA, 25 mM HEPES, and 1% BSA in DPBS (Thermo Fisher Scientific). Flow cytometry analysis was performed using a CytoFLEX benchtop flow cytometer (Beckman Coulter) and analyzed with FlowJo software.

For CD200 staining and cell sorting, single-cell suspensions were stained with an APC-conjugated anti-human CD200 antibody (BioLegend) following the manufacturer's instructions. Briefly, cells were incubated with the antibody at a 1:20 dilution in staining buffer (0.5% BSA in basic culture medium) for 30 mins at 4°C. After staining, cells were sorted using a BD FACSAria Fusion Cell Sorter (BD Biosciences) with DAPI (Sigma-Aldrich) to exclude non-viable cells. The sorted live cells were then plated at a density of 300 cells/μl in 10-20 μl of BME per well in a 48-well cell suspension plate.

For organoid cultures treated with cytokines, flow cytometry sorting was performed on a BD Influx™ cell sorter (BD Bioscience). For organoid cultures infected with the virus, both flow cytometry analysis and sorting were performed on a BD FACSMelody Cell Sorter (BD Biosciences) in a Class II Biosafety Cabinet of an ML-II laboratory.

Transwell culture and HCoV-229E-EGFP infections

Organoids were removed from BME (R&D Systems) and digested with TrypLE (Thermo Fisher Scientific) for 5 minutes into single cells using glass Pasteur pipettes. A total of 200,000 cells were seeded in 500 μL of SMG or SAE culture medium on one well of 12-well ThinCert Tissue Culture Inserts with a 0.4 μm pore size (Greiner), which had been previously coated with 10% BME (R&D Systems). An additional 1.5 mL of medium was added to the bottom chamber of the transwell. After 7-10 days of continuous medium replenishment, the cells formed a confluent layer on the transwell. The medium in the upper chamber of SMG transwell cultures was replaced with DPBS (Thermo Fisher Scientific), while the medium in the upper chamber of SAE transwell cultures was completely removed to establish an air-liquid interface. By Day 21-28, the SMG and SAE transwell cultures had developed into multilayer structures and were ready for further characterization and virus infection experiments.

For infections, transwells were apically exposed to the HCoV-229E-EGFP viral mixture in Advanced Dulbecco's modified Eagle's medium (DMEM)/F12 (Thermo Fisher Scientific) for 16 hours. Viral mixtures were then removed. The upper chambers of transwell cultures were washed with DPBS (Thermo Fisher Scientific) twice. And then, 500 μL of DPBS (Thermo Fisher Scientific) were added to the upper chamber of both SMG and SAE transwell cultures. Culture medium at the bottom chamber of the transwell cultures were replenished. The cultures were then incubated at 33 °C for an additional 24 hours before analysis.

To assess the role of CD13 in HCoV-229E-EGFP infection, SMG organoids were cultured in transwells for 28 days prior to infection. Organoids from three independent donor lines were apically pre-incubated with two different anti-CD13 monoclonal antibodies (clone: WM15, 5μg) (BioLegend, Antibodies) for 1 hour at 37°C prior to viral infection. Following antibody treatment, organoids were infected with HCoV-229E-EGFP at a MOI = 4 and incubated at 33°C for 16 hours in the presence or absence of the blocking antibodies. After incubation, cells were washed, and DPBS with or without the blocking antibodies was added to the apical compartment. After 24 hours post-infection, cells were dissociated and subjected to fluorescence-activated cell sorting to quantify the percentage of HCoV-229E-EGFP-infected cells.

Dot blot

Following the 24-hour incubation period after viral infection, 500 μL of the supernatants were collected. From each sample, 20 μL aliquots of the supernatants were transferred into PCR strip tubes and boiled at 95 °C for 5 minutes. Subsequently, 4 μL of the boiled supernatants were loaded directly onto nitrocellulose membranes and allowed to dry for 5 minutes. The membranes were then blocked with 5% w/v non-fat dry milk in TBST, followed by staining with primary antibodies specific to MUC5B (Atlas Antibodies) or MUC5AC (Thermo Fisher Scientific). This was followed by staining with secondary antibodies: goat anti-rabbit HRP (Thermo Fisher Scientific) or rabbit anti-mouse HRP (Agilent). Finally, the membranes were imaged using the Amersham ImageQuant 800 Western blot imaging system.

Immunohistochemistry staining

Organoids were removed from BME (R&D Systems), washed with DPBS (Thermo Fisher Scientific), and fixed with 4% paraformaldehyde (PFA) for 1 hour at room temperature. Human bronchus tissues were also washed with DPBS (Thermo Fisher Scientific) and fixed with 4% PFA overnight at 4 °C. Both organoids and tissues were then washed, dehydrated using a graded ethanol series, and washed in xylene before being embedded in paraffin. Sections cut from paraffin blocks were stained with antibodies according to the manufacturer's instructions. Slides were imaged using a SLIDEVIEW VS200 Slide Scanner (Olympus). The primary antibodies used for staining paraffin sections included MUC5B (Atlas Antibodies), acetylated alpha Tubulin (Santa Cruz), CD13 (ProteinTech), Human HLA-DR, DP, DQ (BD Biosciences), and MKi-67 (MONOSAN). The secondary antibodies used for staining included EnVision+ Single Reagent (HRP. Mouse) (Agilent) and BrightVision+ Anti-Rabbit IgG (H+L) (Poly-HRP) (Avantor).

Immunofluorescence

Human bronchus tissues, 3D organoids, or transwell cultures were fixed, washed, embedded in tissue freezing medium (Leica Biosystems), and stored at -80 °C. Cryosectioning was performed at -20 °C using a Cryostat (Thermo Fisher Scientific). Sections were then washed and permeabilized in PBST (PBS + 0.1% Tween20). To block non-specific binding, sections were incubated in 10% FBS in PBST. Primary antibodies were applied overnight at 4 °C. The following day, sections were washed and incubated with secondary antibodies at room temperature for 2 hours. Finally, sections were mounted in the Antifade mounting medium (VectorLabs) and analyzed under a confocal microscope.

Confocal Imaging

Sections subjected to immunofluorescence staining were imaged using a Leica Sp8 confocal microscope. Fluorescent images were processed for maximum projection of all z-stacks using Fiji software.

Single-cell transcriptome sample preparation

Organoids were removed from BME (R&D Systems) and digested with TrypLE (Thermo Fisher Scientific) for 5 minutes into single cells using glass Pasteur pipettes. The cells were then washed with ice-cold AdDMEM/F12 (Thermo Fisher Scientific) and resuspended in culture medium supplemented with Y-27632 dihydrochloride (10 μM, Abmole Bioscience). After filtering them into FACS tubes through a cell strainer (Falcon), cells were co-stained with DAPI (Sigma-Aldrich) and DRAQ5 (Biostatus), and subjected to FACS sorting for live cells. FACS was performed on a BD Influx™ cell sorter (BD Biosciences). 4,000 live cells per condition were subjected to droplet-based scRNA-seq using the 10x Genomics platform. Libraries were prepared using the 10x Genomics Chromium 3' Gene Expression solution v3.1 and sequenced on a NovaSeq 6000 (Illumina).

Single-cell RNA-sequencing data processing

Mapping of sequencing reads

The sequencing output was demultiplexed and converted to FASTQ files using the function *mkfastq* from the CellRanger toolkit (v5.0.1). Reads were then mapped to a custom variant of the GRCh38 human transcriptome, and feature count tables were generated using the CellRanger *count* function.

Data pre-processing

CellRanger output files were processed using the Seurat package (v.5.1.0) in R (v.4.3.3). Genes expressed in less than 5 cells were removed. High-quality cells were subsequently obtained by filtering out cells expressing less than 3500 or more than 7500 transcripts, and a mitochondrial gene percentage higher than 5%.

Data integration

Integration of both our organoid datasets (SAE and SMG) was first performed using Reciprocal PCA (RPCA) using the default parameters.[89] After computing PCA dimensions, Uniform Manifold Approximation and Projections (UMAPs) were rendered using dims=1:20. The combined organoid object was subsequently integrated with a previously published human airway tissue dataset from Goldfarbmuren et al.,[21] using RPCA and a k.anchor of 20. Seurat's *IntegrateData* function was used with a k.weight of 80. After integration, t-distributed Stochastic Neighbor Embeddings (t-SNEs) were computed using dims=1:20.

Clustering and differential expression analysis

To determine the cell clusters present, we used the *FindNeighbors* function with dims=1:20, and *FindClusters* with a resolution of 0.3. This yielded 14 clusters. By overlaying these clusters with the original identities assigned by the original metadata of Goldfarbmuren et al.,[21] clusters were annotated. The original *KRT8*^{high} population spanned across four clusters (2, 4, 5, and 11) in our integrated dataset. Two of these clusters (5 and 11) expressed the highest levels of *KRT19* and *SERPINB4*, and were thereby annotated as suprabasal cells.[22] Cluster 4 was annotated as club cells, based on the high expression of club cell markers such as *SCGB1A1*, *SERPINB3*, *CYP2F1*, and *WFDC2*.[90] Finally, cluster 2 showed the highest levels of *KRT8*, thus we assigned this population to *KRT8*^{high} cells. Tissue-labelled differentiating basal cells were found in two of our clusters (0 and 1). Since common basal cell markers (*e.g., IL33*, *TP63*, *KRT5*, and *COL4A5*)[21] were more highly expressed in cluster 0 than in 1, we annotated cluster 0 as "SAE basal" and cluster 1 as "differentiating basal". To distinguish myoepithelial cells in the joint dataset, we calculated a module score[91] using the known myoepithelial cell markers *ACTA2*, *TAGLN*, *CNN1*, *ACTG2*, *LAMA1*, and *FHOD3*.[23,92] The percentage of myoepithelial cells among SMG basal cells was calculated using cells with a module score higher than 0.5. Lastly, to explore cell abundance and gene expression in organoids only, the labels assigned in the integrated object were transferred to the organoid object.

Bulk mRNA sequencing sample preparation

For cytokine treatment experiments, organoids were removed from BME (R&D Systems) and digested with TrypLE (Thermo Fisher Scientific) for 5 minutes to dissociate them into single cells using glass Pasteur pipettes. The cells were then washed with ice-cold AdDMEM/F12 (Thermo Fisher Scientific). For HCoV-229E-EGFP infection experiments, transwell cultures were washed with DPBS and digested with TrypLE (Thermo Fisher Scientific) for 15 minutes, achieving single-cell suspensions through repeated pipetting. The cells were resuspended in culture medium supplemented with Y-27632 dihydrochloride (10 μM, Abmole Bioscience) and stained with CD13-APC antibody (1:250, BioLegend) for 20 minutes at 4 °C. Subsequently, the cells were washed, stained with DAPI (Sigma-Aldrich), and filtered through a cell strainer (Falcon) for sorting. Cells were sorted into 500 μL of TRIzol (Thermo Fisher Scientific) using different gating settings. A range of 25,000 to 150,000 cells were collected and subjected to RNA isolation. For library preparation of bulk RNA sequencing, a minimum of 100 ng of total RNA per condition was utilized. The sequencing library preparation was done by Utrecht Sequencing Facility (USEQ, Utrecht, The Netherlands) using a TruSeq Stranded mRNA polyA kit, and sequenced with Illumina NextSeq2000.

Bulk RNA-sequencing data processing

Raw counts were loaded into R using the *read.csv* function. A DESeq dataset was subsequently created using the DESeq2 package (v.1.42.1), and genes with less than 10 counts across conditions were removed from the matrix. For cytokine treatment experiments, the gene expression profiles of $CD13^+$ cells treated with IL-13 (Peprotech), TNF-α (Peprotech), and IL-1β (Peprotech) were compared to those of untreated $CD13^+$ cells. The top 200 differentially expressed genes were then plotted in a heatmap showing all conditions using the pheatmap package (v.1.0.12). For HCoV-229E-EGFP infection experiments, gene expression in virally infected $CD13^+EGFP^+$ cells were compared to that in non-exposed $CD13^+$ cells or uninfected $CD13^+$ cells, The top 200 differentially expressed genes were thereafter plotted in a heatmap showing all conditions using the package pheatmap (v.1.0.12). Gene ontology analysis was performed using *enrichGO* function of package clusterProfiler (v.4.7.1.002), and the gene set enrichment plot was rendered with the *cnetplot* function.

QUANTIFICATION AND STATISTICAL ANALYSIS

Data are presented as means with standard error of the mean (SEM) to indicate the variation within each experiment. Sample sizes (*n*) presented in this study are all biological replicates. Statistics analysis was performed in Prism 8 and R 4.2.0. Multiple *t*-tests using two-stage linear step-up procedure of Benjamini, Krieger and Yekutieli were used for comparison between two different conditions. For experiments with more than two conditions, ANOVA test was used to calculate significance. Annotation for *P* values in figure legends regardless of statistical test type are: $^*P < 0.05$, $^{**}P < 0.01$, $^{***}P < 0.001$, $^{****}P < 0.0001$.